Final Technical Report

The Effect of Impurities on the Processing of Aluminum Alloys

July 2006

Principal Investigators:

Zi-Kui Liu and Shengjun Zhang
The Pennsylvania State University

Qingyou Han and Vinod Sikka
Oak Ridge National Laboratory

PENNSTATE
1855

OAK RIDGE
National Laboratory
Managed by
UT-Battelle, LLC

FINAL TECHNICAL REPORT

Project Title: The Effect of Impurities on the Processing of Aluminum Alloys

Award No.: DE-FC36-02ID14403

Project Period: September 15, 2002–September 14, 2006

PI: Dr. Zi-Kui Liu
814-865-1934
liu@matse.psu.edu

Authors:

Dr. Zi-Kui Liu	Dr. Qingyou Han
814-865-1934	865-574-4352
liu@matse.psu.edu	hanq@ornl.gov
Shengjun Zhang	Dr. Vinod Sikka
865-574-9956	865-574-5112
sxz142@psu.edu	sikkavk@ornl.gov

Recipient: The Pennsylvania State University
110 Technology Center
University Park, PA 16802
5th Congressional District

Project Team: The Pennsylvania State University

Dr. Zi-Kui Liu	Shengjun Zhang
814-865-1934	865-574-9956
liu@matse.psu.edu	sxz142@psu.edu

National Laboratory: Oak Ridge National Laboratory

Dr. Qingyou Han	Dr. Vinod Sikka
865-574-4352	865-574-5112
hanq@ornl.gov	sikkavk@ornl.gov

Industry Contacts: Dr. Men G. Chu, ALCOA
Dr. Paul Mason, ThermoCalc, Inc.

Contents

List of Figures

List of Tables

Abbreviations and Acronyms

AES	auger electron spectroscopy
Bcc	body-centered cubic
fcc	face-centered cubic
IOF	Industry of the Future
TMS	The Minerals, Metals, and Materials Society
CALPHAD	calculation of phase diagrams
HTE	high-temperature embrittlement
EMF	electromotive force
SQS	special quasirandom structure
SER	Scientific Group Thermodata Europe
hcp	hexagonal close-packed
DFT	density functional theory
LDA	local density approximation
GDA	generalized gradient approximation

Acknowledgments and Disclaimer

Acknowledgments

Disclaimer

Proprietary Data Notice

None

1. Executive Summary

1.1 Research and Development

Calcium, lithium, and sodium are elements that are regarded as impurities in aluminum alloys for automotive applications. During melting and casting, these elements increase melt loss of aluminum alloys [1]. They also increase the hydrogen solubility in the melt and promote the formation of porosity in aluminum castings. During fabrication they affect the hot-shortness and embrittlement [2, 3]. In the 5182 alloy, for instance, a few parts per million of sodium or calcium can lead to cracking during hot rolling. As little as 10 ppm calcium or lithium in 5XXX welding wire causes the weld arc to be unstable [4]. These elements also affect corrosion behavior [5]. Although these elements have been identified as harmful impurities for the extrusion aluminum alloys, no systematic research has been carried out to investigate the behavior of these impurities during the processing of aluminum alloys.

For this Aluminum Industry of the Future (IOF) project, the effect of impurities on the processing of aluminum alloys was systematically investigated. The work was carried out as a collaborative effort between the Pennsylvania State University and Oak Ridge National Laboratory. Industrial support was provided by ALCOA and ThermoCalc, Inc. The achievements described below were made.

A method that combines first-principles calculation and calculation of phase diagrams (CALPHAD) was used to develop the multicomponent database Al-Ca-K-Li-Mg-Na. This method was extensively used in this project for the development of a thermodynamic database. The first-principles approach provided some thermodynamic property data that are not available in the open literature. These calculated results were used in the thermodynamic modeling as experimental data. Some of the thermodynamic property data are difficult, if not impossible, to measure. The method developed and used in this project allows the estimation of these data for thermodynamic database development.

The multicomponent database Al-Ca-K-Li-Mg-Na was developed. Elements such as Ca, Li, Na, and K are impurities that strongly affect the formability and corrosion behavior of aluminum alloys. However, these impurity elements are not included in the commercial aluminum alloy database. The process of thermodynamic modeling began from Al-Na, Ca-Li, Li-Na, K-Na, and Li-K sub-binary systems. Then ternary and higher systems were extrapolated because of the lack of experimental information. Databases for five binary alloy systems and two ternary systems were developed. Along with other existing binary and ternary databases, the full database of the multicomponent Al-Ca-K-Li-Mg-Na system was completed in this project. The methodology in integrating with commercial or other aluminum alloy databases can be developed.

The mechanism of sodium-induced high-temperature embrittlement (HTE) of Al-Mg is now understood. Using the thermodynamic database developed in this project, thermodynamic simulations were carried out to investigate the effect of sodium on the HTE of Al-Mg alloys. The simulation results indicated that the liquid miscibility gap resulting from the dissolved sodium in the molten material plays an important role in HTE. A liquid phase forms from the solid face-centered cubic (fcc) phase (most likely at grain boundaries) during cooling, resulting in the occurrence of HTE. Comparison of the thermodynamic simulation results with experimental measurements on the high-temperature ductility of an Al-5Mg-Na alloy shows that HTE occurs in the temperature range at which the liquid phase exists. Based on this fundamental understanding of the HTE mechanism during processing of aluminum alloy, an HTE sensitive

zone and a hot-rolling safe zone of the Al-Mg-Na alloys are defined as functions of processing temperature and alloy composition. The tendency of HTE was evaluated based on thermodynamic simulations of the fraction of the intergranular sodium-rich liquid phase. Methods of avoiding HTE during rolling/extrusion of Al-Mg-based alloys were suggested.

Energy and environmental benefits from the results of this project could occur through a number of avenues: (1) energy benefits accruing from reduced rejection rates of the aluminum sheet and bar, (2) reduced dross formation during the remelting of the aluminum rejects, and (3) reduced CO_2 emission related to the energy savings. The sheet and extruded bar quantities produced in the United States during 2000 were 10,822 and 4,546 million pounds, respectively. It is assumed that 50% of the sheet and 10% of the bar will be affected by implementing the results of this project. With the current process, the rejection rate of sheet and bar is estimated at 5%. Assuming that at least half of the 5% rejection of sheet and bar will be eliminated by using the results of this project and that 4% of the aluminum will be lost through dross (Al_2O_3) during remelting of the rejects, the full-scale industrial implementation of the project results would lead to energy savings in excess of 6.2 trillion Btu/year and cost savings of \$42.7 million by 2020.

1.2   Technology Transfer

Intellectual property has been generated from this significant effort. A thermodynamic database has been developed. The thermodynamic database covers aluminum alloys containing Na, Ca, Mg, Li, and K, most of which are not included in commercial thermodynamic databases. The research team is working with the Pennsylvania State University and interacting with ThermoCalc, Inc. on copyright and license issues.

1.3   Commercialization

This project was conducted in response to a call for proposals under the Aluminum IOF, Industrial Technologies Program of the U.S. Department of Energy. The goal was to understand the effect of impurities on the processing of aluminum alloys. This study focused on developing a thermodynamic database of aluminum containing Ca, Na, and Li; studying phase transformations and segregation of these impurities during processing; validating the modeling predictions through experimental observations; and implementing database and calculation procedures for industrial practice. Project participants have used several mechanisms to inform industries of the research results and advance commercialization, including (1) incorporating the results into a commercial thermodynamic database so the aluminum industry can obtain access to the project results and (2) making presentations at national meetings organized by the Minerals, Metals, and Materials Society (TMS) and the American Society of Metals as well as at industrial locations.

Companies who have expressed interest in the research results of this project include ALCOA, Aleris International, Secat, Inc, Indalco, Novelis, and ThermoCalc, Inc. In particular, ThermoCalc, Inc. is evaluating the database developed in this project and incorporating it into its commercial database.

1.4   Recommendations

Future studies should determine the mechanism of sodium-induced HTE in Mg-Li and Al-Li alloys. The database of the Al-Li-Na and Mg-Li-Na system will be developed first. It is recommended that more impurity elements then be added into the database.

2. Introduction

Aluminum alloys are widely used in the automobile and aerospace industries as structural materials because of their light weight, high strength, and good formability. However, they suffer from the poor hot-rolling characteristics because of undesired impurities such as calcium, potassium, lithium, and sodium. These impurity elements increase the hydrogen solubility in the melt and promote the formation of porosity in aluminum castings. During fabrication of aluminum alloys, they cause hot-shortness and embrittlement because of cracking [2, 3]. They also lead to "blue haze" corrosion, which promotes the discoloration of aluminum under humid condition [4, 5]. The removal of these elements increases overall melt loss of aluminum alloys when aluminum products are remelted and recast [1].

Sodium is one of the common impurities in the aluminum and magnesium alloys. In industry, primary aluminum is produced by the Hall-Héroult process through the electrolysis of the mixture of molten alumina and cryolite (Al_2O_3+Na_3AlF_6), the latter being added to lower the melting point [6]. Therefore, aluminum without further treatment inevitably contains some sodium (>0.002%), and the content of sodium in aluminum is influenced by the thermodynamics and kinetics of the electrolysis. Similarly, in the electrolytical production and subsequent processing of magnesium, magnesium is commonly in contact with molten salts of mixture of NaCl and $MgCl_2$. Because of the exchange reaction shown as Eq.(1), 2 to 20 ppm of sodium is often found in magnesium alloys [7]. (*Note:* ppm is expressed as wt ppm hereafter unless otherwise specified.)

$$2NaCl(l) + Mg(l) \rightarrow 2Na(l) + MgCl_2(l) \qquad (1)$$

Besides origination from the industry production process, part of the sodium can be introduced from the alumina crucible by the reaction between the molten Al-Mg alloys and Na_2O impurity of the alumina crucible in laboratory experiments [3]. The tracer element potassium plays a role similar to that of sodium in aluminum alloys, although it is seldom discussed.

No systematic theoretic research has been carried out to investigate the behavior of these impurities during the processing of aluminum alloys. A thermodynamic description of the Al-Ca-K-Li-Mg-Na system is needed to understand the effects of Ca, K, Li, and Na on phase stability of aluminum alloys.

As the first step of the thermodynamic description of the high-order system, the sub-binary systems were modeled in this project using the CALPHAD technique combined with first-principles calculations. Then, ternaries and higher-order systems could be modeled. For the ternaries without experimental data, the thermodynamic description was extrapolated by combining the sub-binary systems.

3. Background

3.1   High-Temperature Embrittlement (HTE)

As a result of good formability, the Al-5%Mg alloys are being developed and widely used in the automotive industry. (*Note:* % stands for wt % hereafter unless otherwise specified.) However, they suffer from poor hot-rolling characteristics. Sodium is among the detrimental impurities that lead to HTE at temperatures of 473 to 673 K because of intergranular fracture and formation of cracks during hot rolling [2, 3].

Despite numerous investigations, the mechanisms of sodium on HTE of Al-5%Mg alloys are still controversial [8, 9]. No detailed investigations were carried out to reveal the correlations between HTE, phase relations, temperature, and sodium content of Al-5%Mg alloys. In this work, efforts were made to investigate these relationships through thermodynamic modeling of the Al-Mg-Na system and to clarify the mechanisms of HTE caused by sodium in Al-5%Mg alloys.

Besides sodium, it was reported that calcium and lithium lead to HTE in Al-Mg alloys, though their detrimental effects are much milder than those of sodium [10, 11]. It was also found that sodium and potassium cause HTE in Al-Li alloys, which reduces their toughness and ductility by forming discrete lenticular liquid particles along grain boundaries [12, 13].

3.2   Computational Materials Science

In the development of alloys with better properties to meet today's increasingly demanding applications, the traditional experimental trial-and-error approach becomes more and more insufficient because most commercial alloys are multicomponent in nature and can contain as many as ten alloying elements. It is impractical to explore such a high-dimensional-composition space by experimental means. Fortunately, with rapidly increasing computing power, it is now possible to use computers to predict the properties of alloys before doing experiments.

Based on computational thermodynamics, the CALPHAD approach has been very successful in modeling phase equilibriums and phase transformations in multicomponent alloys. Commercial computer programs like Thermo-Calc and DICTRA have been widely used for such purposes, along with sophisticated thermodynamic and kinetic databases developed using the CALPHAD approach.

First-principles calculations based on density functional theory are now routinely used to predict the thermodynamic, structural, magnetic, electrical, and optical properties of a wide range of materials. Using only the atomic number and atom positions as input, the total energy of a crystal structure can be accurately calculated, and the relative lattice stability between two different crystal structures and the formation energy of a compound can be evaluated at 0 K. Many software packages, such as VASP, LKKR, and WIEN2K, are available.

3.3 Research Objective and Report Outline

The objective of the present work is to understand the effect of impurities such as Ca, Li, K, and Na on aluminum-alloys processing through thermodynamic modeling and calculations.

A thermodynamic database is the key to and basis for this work. Because Ca, Li, K, and Na impurity elements are not included in the existing aluminum database, thermodynamic description of the Al-Ca-K-Li-Mg-Na system was carried out at first using CALPHAD and first-principles approaches. All the available experimental data in the literature were reviewed, including phase-equilibrium and thermochemical data. The formation enthalpies of phases were provided using the first-principles method if experimental ones were not available. Special quasirandom structures (SQSs) were applied to model the substitutionally random alloys. The new database will integrate with the commercial aluminum databases, making it a more powerful tool for helping solving many industry problems.

In Chapter 4, the methodology is introduced in detail, including the CALPHAD approach and first-principles method. Chapter 5 provides the results from first-principles calculations and a discussion of them. The development of the thermodynamic database of the Al-Ca-Li-Mg-Na quinary system is presented in Chapter 6, followed by thermodynamic investigation of the effect of sodium on HTE in Al-Mg alloys in Chapter 7, accomplishments in Chapter 8, and Summary in Chapter 9. Finally, Chapter 10 discusses recommended future work.

4. Methodology

4.1   CALPHAD Approach

Phase diagrams are a fundamental tool for materials scientists. They represent the equilibrium state of a system as a function of composition, temperature, and pressure. They are useful roadmaps for material design and processing. Nevertheless, experimental determinations of phase diagrams are very costly and time-consuming. The CALPHAD approach was introduced by Kaufman [14, 15] to model complex phase equilibriums in multicomponent alloys. Its theoretical basis is modeling of individual phases; given the Gibbs energies of all the competing phases in a system, the final equilibrium state at a given composition, temperature, and pressure can be calculated by minimizing the total Gibbs energy of the system as follows:

$$G = \min\left(\sum_p n_p G_p \right), \tag{2}$$

where n_p is the number of moles of phase $p,$ and G_p is its Gibbs energy. By intentionally keeping the stable phases from appearing, metastable phase equilibrium can also be calculated. CALPHAD modeling of a multicomponent system is built from lower-order systems such as pure elements and binary and ternary systems as discussed below.

4.1.1   Pure Elements

The Gibbs energies of pure elements in their stable, metastable, or even unstable states, the so-called "lattice-stabilities," are taken from the Scientific Group Thermodata Europe (SGTE) pure element database [16]. The reference state is chosen to be the enthalpies of the pure elements in their stable states at 298.15 K and 1 bar, commonly referred to as the stable element reference (SER). In the SGTE pure elements database, the thermodynamic function of a pure element is usually described as shown in Eq. (3) below.

$$^{o}G_i^m - H_i^{SER} = a + bT + cT \ln T + \sum d_n T^n \tag{3}$$

The left-hand term is defined as the Gibbs energy relative to the SER state, where H_i^{SER} is the enthalpy of the element in its SER state at 298.15 K; a, b, c, and d_n are coefficients; and n represents a set of integers, typically taking the values of 2, 3 and -1. From Eq. (3) other thermodynamic properties of interest can be obtained as shown in Eqs. (4), (5), and (6) below..

$$S = -\left(\frac{\partial G}{\partial T} \right)_p = -b - c - c \ln T - \sum n d_n T^{n-1} \tag{4}$$

$$H = G + TS = a - cT - \sum (n-1) d_n T^n \tag{5}$$

$$C_p = \left(\frac{\partial H}{\partial T} \right)_p = -c - \sum n(n-1) d_n T^{n-1} \tag{6}$$

6

4.1.2 Stoichiometric Compounds

For stoichiometric compounds, when experimental heat capacity data are available, it is preferable to express their Gibbs energies directly referred to the SER in the similar form as Eq. (2) as shown in Eq. (7) below.

$$^{o}G_m^{A_{1-x}B_x} - (1-x)H_A^{SER} - xH_B^{SER} = a + bT + cT\ln T + \sum d_n T^n \qquad (7)$$

For compounds without heat capacity data, the Neumann-Kopp rule is used (i.e., assuming $\Delta C_p = 0$). Their Gibbs energies can be expressed as

$$^{o}G_m^{A_{1-x}B_x} = (1-x)^{o}G_A^{\Phi_A} + x^{o}G_B^{\Phi_B} + a + bT, \qquad (8)$$

where $^{o}G_i^{\Phi}$ is the molar Gibbs energy of pure element i in its structure Φ, and a and b are the enthalpy and entropy of formation of the compound with respect to A and B in their structures Φ_A and Φ_B, respectively.

4.1.3 Solution Phases

For solution phases such as liquid, fcc, body-centered cubic (bcc) and hexagonal close-packed (hcp), the substitutional random solution model is usually used. For a binary A–B solution phase Φ, for example, the Gibbs energy is written as

$$G_m^{\Phi} = \sum_i x_i {}^{o}G_i^{\Phi} + RT\sum_i x_i \ln x_i + {}^{xs}G_m^{\Phi}, \qquad (9)$$

where $^{o}G_i^{\Phi}$ is the molar Gibbs energy of the pure element i with the structure Φ from Dinsdale [16], and R is the gas constant. The first term on the right side is the contribution of the pure components of the phase to the Gibbs energy, the second term is the ideal mixing contribution, and $^{xs}G_m^{\Phi}$ is the excess Gibbs energy resulting from non-ideal interactions between the components, expressed in the Redlich-Kister polynomial [17] as shown in Eq. (10) below.

$$^{xs}G_m^{\Phi} = \sum_i \sum_{j>i} x_i x_j \sum_{k=0}^{n} {}^{k}L_{i,j}^{\Phi}(x_i - x_j)^k + x_i x_j x_h I^{\Phi}, \qquad (10)$$

where $^{k}L_{i,j}^{\Phi}$ is the kth binary interaction parameter between i and j and can depend on temperature as $^{k}A_k^{\Phi} + {}^{k}B_k^{\Phi}T + {}^{k}C_k^{\Phi}\ln T$, with $^{k}A_k^{\Phi}$, $^{k}B_k^{\Phi}$, and $^{k}C_k^{\Phi}$ being model parameters to be evaluated. I^{Φ} is the ternary interaction parameter expressed as

$$I^{\Phi} = x_i {}^{0}L_i + x_j {}^{1}L_j + x_h {}^{2}L_h, \qquad (11)$$

where $^{0}L_i$, $^{1}L_j$, and $^{2}L_h$ represent ternary interaction parameters.

4.1.4　Ionic Liquid Phase

The liquid phase with ionic species can be described by a two sublattice ionic model, proposed by Hillert et al. [18] and modified by Sundman [19]. The formula for the sublattice ionic liquid is given by $\left(C_i^{+v_i}\right)_P\left(A_j^{-v_j},Va,B_k^0\right)_Q$, where C and A are cations and anions, respectively; Va and B are vacancies and neutral species; and v is the valence. P and Q are the number of sites of the sublattices and defined by electric neutrality as shown in Eqs. (12) and (13) below.

$$P = \sum_j v_j y_{A_j} + Q y_{Va} \tag{12}$$

$$Q = \sum_i v_i y_{C_i} \tag{13}$$

In general, the total Gibbs energy for the two-sublattice ionic liquid model is represented by

$$
\begin{aligned}
G_m^{Liq} =& \sum_i \sum_j y_{C_i} y_{A_j} G_{C_i:A_j}^{Liq} + Q y_{Va} \sum_i y_{C_i} G_{C_i}^{Liq} + Q \sum_k y_{B_i} G_{B_i}^{Liq} \\
&+ RT\left[P \sum_i y_{C_i} \ln y_{C_i} + Q\left(\sum_j y_{A_j} \ln y_{A_j} + y_{Va} \ln y_{Va} + \sum_k y_{B_k} \ln y_{B_k} \right) \right] \\
&+ \sum_{i_1}\sum_{i_2}\sum_j y_{C_{i_1}} y_{C_{i_2}} y_{A_j} L_{C_{i_1},C_{i_2}:A_j} + \sum_{i_1}\sum_{i_2} y_{C_{i_1}} y_{C_{i_2}} y_{Va} L_{C_{i_1},C_{i_2}:Va} \\
&+ \sum_i\sum_{j_1}\sum_{j_2} y_{C_i} y_{A_{j_1}} y_{A_{j_2}} L_{C_i:A_{j_1},A_{j_2}} + \sum_i\sum_j y_{C_i} y_{A_j} y_{Va} L_{C_i:A_j,Va} \\
&+ \sum_i\sum_j\sum_k y_{C_i} y_{A_j} y_{B_k} L_{C_i:A_j,B_k} + \sum_i\sum_k y_{C_i} y_{B_k} y_{Va} L_{C_i:Va,B_k} + \sum_{k_1}\sum_{k_2} y_{B_{k_1}} y_{B_{k_2}} L_{B_{k_1},B_{k_2}},
\end{aligned}
\tag{14}
$$

where G_X is the Gibbs energy of species X. The terms in the first row give the reference state, those in the second row the ideal Gibbs energy of mixing, and the rest of the rows the excess Gibbs energy of mixing. In the third row, $L_{i_1,i_2:j}$ is an interaction parameter representing the interaction between two cations (denoted by i) and a common anion (denoted by j).

The final term, summing interactions between neutral species, is of special note because it is the only term that involves interactions on only one sublattice. For the calculation of the interaction parameter between neutral species, effects of cations are ignored, and only interactions among the neutral species are considered.

4.1.5　Modeling Procedures

As illustrated in Fig. 4.1, the development of thermodynamic databases using the CALPHAD approach is usually carried out in the following four steps:

1. Do a thorough search for all available experimental data in the literature (e.g., thermochemical and phase-equilibrium data) of the system to be studied. When experimental data are insufficient, first-principles results can be used as if they were from experiments.

```
┌─────────────────────┐   ┌─────────────────────┐   ┌─────────────────────┐
│  Experimental Data  │   │   First-Principles  │   │  Experimental Data  │
│ —Phase Equilibrium  │   │    Calculations     │   │ —Tracer Diffusivity │
│  —Thermochemical    │   │    —ΔH at 0 K       │   │ —Chemical Diffusivity│
└─────────────────────┘   └─────────────────────┘   └─────────────────────┘
                          ┌────────────────────┐
                          │  Model Parameter   │
                          │     Evaluation     │
                          └────────────────────┘
        ┌──────────────────────────┐   ┌──────────────────────┐
        │  Thermodynamic Database  │   │   Mobility Database   │
        └──────────────────────────┘   └──────────────────────┘
┌─────────────────┐   ┌─────────────────────┐   ┌─────────────────────┐
│  Multicomponent │   │ Scheil Simulation of│   │  Simulation of Phase│
│ Phase-Equilibrium│  │  Non-equilibrium    │   │   Transformation    │
│   Calculations  │   │   Solidification    │   │      —DICTRA        │
│                 │   │of Multicomponent    │   │    —Phase Field     │
│                 │   │      Alloys         │   │                     │
└─────────────────┘   └─────────────────────┘   └─────────────────────┘
                      ┌─────────────────────┐
                      │ System Materials    │
                      │      Design         │
                      └─────────────────────┘
```

Fig. 4.1. Flowchart of computational materials science via CALPHAD and first-principles methods.

2. Critically assess the validity of each piece of data and assign it a certain weight according to its experimental uncertainty and relative importance.
3. Based on the crystal structure information, choose a suitable thermodynamic model to represent each of the phases in the system. Such models generally include some unknown phenomenological model parameters that need to be determined.
4. Adjust the unknown model parameters to obtain the best possible fit between model calculations and experimental data.

The final model parameters are stored in computerized databases. Once the Gibbs energies of all the constituent subsystems have been assessed, those data can be combined to predict phase equilibriums in higher-order systems.

4.2 First-Principles Method

4.2.1 Fundamentals

Theoretically, an exact treatment of solids can be obtained by solving the following many-body Schrödinger equation involving both the nuclei and the electrons:

$$\hat{H}\psi(\vec{R}_1,\vec{R}_2,\cdots\vec{R}_N,\vec{r}_1,\vec{r}_2,\cdots\vec{r}_n) = E\psi(\vec{R}_1,\vec{R}_2,\cdots\vec{R}_N,\vec{r}_1,\vec{r}_2,\cdots\vec{r}_n),$$ (15)

where $\vec{R}_I$ s are the nuclei coordinates, $\vec{r}_i$ s are the electron coordinates, $\hat{H}$ is the Hamiltonian operator, E is the total energy of the system, N is the total number of nuclei, and n is the total number of electrons in the system.

However, although theoretically exact, it is impossible to solve Eq. (15) because of its many-body nature and the limits of current computing power. In fact, the only system that can be solved analytically is the single-electron hydrogen atom. In general, the Schrödinger equation has to be solved numerically through a series of approximations. In the following sections, several levels of approximations will be briefly introduced.

4.2.1.1 Born-Oppenheimer approximation

Because the nuclei are much heavier than the electrons, it can be assumed that the electrons are always in instantaneous ground state with the nuclei. In other words, we can fix the positions of the nuclei and only solve the many-body Schrödinger equation for the electrons as shown in Eq. (16) below.

$$\hat{H}\psi(\vec{r}_1,\vec{r}_2,\cdots\vec{r}_n) = E\psi(\vec{r}_1,\vec{r}_2,\cdots\vec{r}_n)$$ (16)

Because the nuclei are "frozen," they contribute to only an external potential for the electrons.

4.2.1.2 Density functional theory

Even after the simplification by the Born-Oppenheimer approximation, the Schrödinger equation in essence is still a many-body problem because of the interactions between electrons; each electron will interact with every other electron in the system. Most modern electronic calculations for solids are based on the density functional theory (DFT) proposed by Kohn and Sham [20]. According to DFT, the total energy of a system can be uniquely defined by the electron charge density (i.e., $E = E[\rho(\vec{r})]$). The original many-electron Schrödinger equation is then converted into a set of one-electron Schrödinger equations, one for each electron in the system, as shown in Eq, (17) below.

$$\left[-\frac{\hbar^2}{2m_e}\nabla_i^2 - \frac{e^2}{4\pi\varepsilon_0}\sum_{I=1}^{N}\frac{Z_I}{|\vec{r}-\vec{R}_I|} + \frac{e^2}{4\pi\varepsilon_0}\int\frac{\rho(\vec{r}')}{|\vec{r}-\vec{r}'|}d^3\vec{r}' + V_{XC}[\rho(\vec{r}')]\right]\psi_i(\vec{r}) = \varepsilon_i\psi_i(\vec{r})$$ (17)

The exchange correlation potential $V_{XC}[\rho(\vec{r}')]$ is given by the functional derivative shown in Eq. (18).

$$V_{XC}[\rho(\vec{r}')] = \frac{\delta}{\delta\rho(\vec{r}')} E_{XC}[\rho(\vec{r})]$$ (18)

Nevertheless, the exact form of the exchange correlation energy $E_{XC}[\rho(\vec{r})]$ is unknown. The most widely used approximation is the so-called local density approximation (LDA), which assumes that the exchange correlation energy $E_{XC}[\rho(\vec{r})]$ is only a function of the local charge density in the form of

$$E_{XC}[\rho(\vec{r})] = \int \rho(\vec{r})\varepsilon_{XC}[\rho(\vec{r})]d^3\vec{r},$$ (19)

where $\varepsilon_{XC}[\rho(\vec{r})]$ is the exchange-correlation energy of homogeneous electron gas of the same charge density. LDA is expected to work well for systems with a slowly varying charge density, but surprisingly, LDA works quite well for realistic systems as well.

One significant limitation of LDA is its over-binding of solids; lattice parameters are usually under predicted, while cohesive energies are usually over predicted. In an effort to rectify the inaccuracies of LDA, the generalized gradient approximation (GGA) was introduced. GGA is a natural improvement on LDA because it considers not only the local charge density, but also its gradient. The lattice parameters calculated by GGA generally agree noticeably better with experiments than LDA. It is worth noting here that there is only one LDA exchange correlation functional (i.e., the one by Ceperley and Alder [21]). Nevertheless, many versions of GGA exist because of the freedom in how the gradient term is incorporated in the exchange correlation energy.

The actual first-principles total energy calculations are performed in a self-consistent cycle. We first "guess" the initial charge density function. By solving Eq. (17), a new charge density is obtained. This loop is repeated until the new charge density (or the new total energy) does not differ much from the old one (i.e., the iteration has converged). In practice, the nuclei also need to be relaxed into their equilibrium positions such that the quantum-mechanical forces acting on each of them vanish. Such structural relaxations are usually performed using a conjugate-gradient or a quasi-Newton scheme. The final obtained total energies can be used to extract the formation enthalpies of stable, metastable, or even unstable structures at T = 0 K using the following equation:

$$\Delta H(A_{1-x}B_x) = E(A_{1-x}B_x) - (1-x)E(A) - xE(B),$$ (20)

where Es are the first-principles calculated total energies of structure $A_{1-x}B_x$ and pure elements A and B, each fully relaxed to their equilibrium (zero-pressure) geometries, respectively.

4.2.2   Treating Disordered Alloys via Special Quasirandom Structures

Because first-principles DFT calculations rely on the construction of cells with periodic boundary conditions, the calculations are fairly straightforward for perfectly ordered stoichiometric compounds. However, the situation is more complicated when treating disordered alloys.

One way to treat random $A_{1-x}B_x$ solid solutions would be to directly construct a large super cell and randomly decorate the host lattice with A and B atoms. Such an approach would necessarily require very large super cells to adequately mimic the statistics of the random alloys. Because density-functional methods are computationally constrained by the number of atoms that one can treat, this brute-force approach could be computationally prohibitive. The concept of SQSs proposed by Zunger et al. [22-24] aims to overcome the limitations of mean-field theories, but without the prohibitive computational cost associated with directly constructing large super cells with random occupancy of atoms. SQSs are specially designed small-unit-cell periodic structures with only a few (approximately 2 to 32) atoms per unit cell that closely mimic the most relevant, near-neighbor pair and multisite correlation functions of the random substitutional alloys. Because the SQS approach is not a mean-field one, a distribution of distinct local environments is maintained, the average of which corresponds to the random alloy. Thus, a single DFT calculation of an SQS can reveal many important alloy properties (e.g., equilibrium bond lengths, charge transfer, formation enthalpies) that depend on the existence of those distinct local environments. Furthermore, because the SQS approach is geared toward relatively small unit cells, essentially any DFT method can be applied to this approach that is capable of accurately capturing the effects of atomic relaxation.

The SQS approach has been used extensively to study the enthalpies of formation, bond length distributions, density of states, band gaps, and optical properties in semiconductor alloys [22-24]. It has also been used to investigate the local lattice relaxations in size-mismatched transition metal alloys [25-28] and to predict the formation enthalpies of aluminum-based fcc alloys [29]. However, to date, most applications of the SQS methodology have been for systems in which the substitutional alloy problem is fcc-based (e.g., fcc-based metals, zinc-blend-based semiconductors, or rock-salt-based oxides). Jiang *et al.* [30] developed SQSs for binary bcc alloys at compositions $x = 0.25$, 0.50, and 0.75, respectively. Because these SQSs are quite general, they can be applied to any binary bcc solutions.

5. First-Principles Calculations

Enthalpy of mixing in solid solutions is typically not available, particularly for binary systems with intermediate phases or a miscibility gap, where solubility ranges are usually rather limited. The corresponding interaction parameters in those solution phases have large uncertainties. In the present work, enthalpies of mixing of bcc phases in the Ca-Li, Ca-Na, Li-Na, and K-Na systems were predicted by first-principles calculations. For the purpose of validation, the enthalpy of formation of KNa_2 was also calculated and compared with experimental data.

First-principles calculations were performed using the Blöchl's projector-augmented-wave approach [31, 32] as implemented in the highly-efficient Vienna *Ab-initio* Simulation Package [33, 34]. The generalized gradient approximation [35] was adopted in the present study. The k-point meshes for Brillouin-zone sampling were constructed using the Monkhorst–Pack scheme [36], and the total number of k-points times the total number of atoms per unit cell was at least 6000.

The present study used the 16-atom bcc SQSs developed by Jiang et al. [30]. The researchers fully relaxed the unit cell volume and all the internal atomic positions of the SQSs in their calculations.

The enthalpies of mixing in bcc of an A-B system are calculated as follows:

$$\Delta H_{mix}^{bcc}(A_{1-x}B_x) = E^{bcc}(A_{1-x}B_x) - (1-x)E^{bcc}(A) - xE^{bcc}(B), \quad (21)$$

where x is the molar fraction of B being at 0.25, 0.50, and 0.75, respectively, and Es are the total energies of the bcc-SQS, bcc-A, and bcc-B at 0 K, each relaxed to their equilibrium geometries to minimize their total energies, respectively. All the bcc-SQS results are shown in Table 5.1 and Fig. 5.1.

The enthalpy of formation of the compound KNa_2 is calculated as follows:

$$\Delta_f H^{KNa_2} = E(KNa_2) - E^{bcc}(K) - 2E^{bcc}(Na), \quad (22)$$

where Es are the total energies of KNa_2, bcc-K and bcc-Na at 0 K, each relaxed to their equilibrium geometries to minimize their total energies, respectively.

Table 5.1. The results of first-principles calculations compared to experimental data in the K-Na system

| Phase | Composition | Total Energy (ev/atom) | Enthalpy (J/mol of atom) | | | Lattice Constant (Å) | | |
| | | | Calculated | Experimental | | Calculated | Experimental | |
				Value	Reference		Value	Reference
K	100 at. % K	−1.0384	0	—	—	5.271	5.328 (298 K)	[37]
Na	100 at. % Na	−1.3165	0	—	—	4.197	4.2820 ± 0.0005 (293 K)	[38]
KNa$_2$	66.7 at. % Na	−1.2238	−699	−606.68	[39]	a = 7.394 c = 12.083	a = 7.50 c = 12.31	[40]
Bcc (K-Na)	25 at. % Na	−1.1589	1786	—	—	5.026	—	—
	50 at. % Na	−1.1464	2994	—	—	4.763	—	—
	75 at. % Na	−1.1525	2408	—	—	4.508	—	—
Bcc (Ca-Na)	25 at. % Na		3020	—	—		—	—
	50 at. % Na		4943	—	—		—	—
	75 at. % Na		4367	—	—		—	—
Bcc (Ca-Li)	25 at. % Li		3376	—	—		—	—
	50 at. % Li		5395	—	—		—	—
	75 at. % Li		4948	—	—		—	—
Bcc (Li-Na)	25 at. % Na		3765	—	—		—	—
	50 at. % Na		4726	—	—		—	—
	75 at. % Na		3016	—	—		—	—
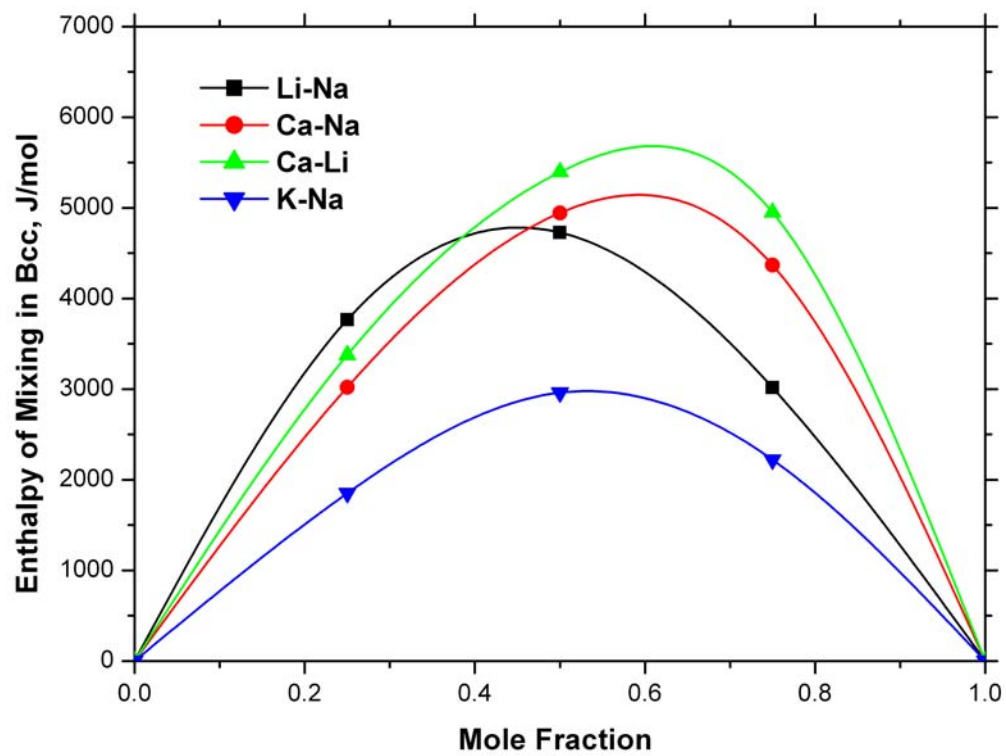
Fig. 5.1. Results via first-principles calculations about the bcc solution phases.

6. Development of the Thermodynamic Database of the Al-Ca-Li-Mg-Na System

6.1 Experimental Data and Previous Modeling

There are 15 binary subsystems in the Al-Ca-K-Li-Mg-Na system. Six of them were modeled by others, including the Al-Ca system modeling by Ozturk et al. [41], the Al-Mg system modeled by Liang et al. [42], the Ca-Li system modeled by Grobner et al. [43], the Ca-Mg system done by Zhong in the researchers' group, and the Al-Li and Mg-Li systems taken from COST2 database. All these subsystems are accepted in the present work. Five of them associated with Na (i.e., Al-Na, Ca-Na, K-Na, Li-Na, and Mg-Na) are modeled in the present work. The other four associated with K (i.e., Al-K, Ca-K, Li-K, and Mg-K) are for future work.

There are 20 ternary subsystems in the Al-Ca-K-Li-Mg-Na system. Only one of them, the Al-Mg-Ca ternary system, has experimental information and was modeled by others in the researchers' group. The ternary interactions are not considered in others ternary systems.

In this section, all available experimental data of the binary systems (Al-Na, Ca-Na, K-Na, Li-Na and Mg-Na) in the literature are critically reviewed, including both phase-equilibrium and thermochemical data.

6.1.1 Al-Na System

Available phase-equilibrium experimental works of the Al-Na binary system were focused on the aluminum-rich region. Great efforts were made to investigate the solubility of sodium in liquid aluminum.

Heycock and Neville [44] investigated the lowering of the freezing point of sodium by addition of many other metals and found that aluminum and sodium do not mix. Mathewson [45] found thermal arrests at temperatures indistinguishable from the melting point of the pure aluminum and sodium. The temperatures of invariant reactions were first determined to be 930 K and 370.5 K. However, the results were affected by the low purity of aluminum (99.7% aluminum). Scheuer [46] measured the solubility of sodium in liquid aluminum by heating aluminum with an excess of sodium under hydrogen until equilibrium was attained, followed by quenching the melt and determining the sodium content of the aluminum -rich layer. The solubility of sodium was pointed out to be 0.10 at. % at 973 K, 0.115 at. % at 1023 K, and 0.128 at. % at 1073 K. As a result of hydrogen contamination, the results are rather uncertain, as pointed out by Murray [47].

Fink, Willey, and Stumpf [48] determined the boundary of the liquid miscibility gap by a method similar to that of Scheuer [46] except under argon instead of hydrogen. They determined the monotectic temperature and the hypo-monotectic liquidus using both direct and differential thermal analysis techniques. Their results show that the monotectic reaction is at 932 K, with the liquid composition being 0.18 at. % sodium, and the solubility of sodium in liquid aluminum decreases slightly with increasing temperature. They also found the maximum solubility of sodium in solid aluminum to be less than 0.003 at. % using electrical resistivity measurement

and metallographic examination. However, their results about the retrograde solubility of sodium in liquid aluminum seem unreasonable.

Ransley and Neufeld [49] redetermined the boundary of the liquid miscibility gap and the solid solubility of sodium in aluminum. They immersed high-purity aluminum (aluminum >99.99 at. %) into liquid sodium and let it get saturated (up to 650 h) in a stout mild-steel bomb. Afterwards the specimens were removed from the furnace and allowed to cool freely in air. The amount of sodium dissolved in aluminum was investigated by chemical analysis. The solid solubility of sodium in aluminum was found to be approximately 0.002 at. % in the range of 923–933 K. The monotectic composition was found to be 0.14 at. % sodium at 932 K, and the solubility of sodium in liquid aluminum increased smoothly with increasing temperature. Their results were given higher weight in the present work because they avoided the drawbacks of the previous works [45, 46, 48].

More recently, Hansen, Tuset, and Haarberg [50] determined the maximum solubility of sodium in solid aluminum using electromotive force (EMF) measurements and quenching experiments. Their results showed the composition of saturated sodium in liquid aluminum to be 1.348 at. % at 1023 K, 0.7639 at. % at 1073 K, and 0.6610 at. % at 1123 K, which are more than ten times higher than the values reported previously [46, 48, 49]. Furthermore, their results indicated that Al-Na exhibits a large retrograde solubility. Hansen, Tuset, and Haarberg derived an equation based on Fick's law by assuming that saturation is controlled by diffusion of sodium into liquid aluminum. According to their calculated results from their derived equation, Hansen, Tuset, and Haarberg concluded that saturation was probably never reached in previous attempts [46, 48, 49] to determine the solubility of sodium in liquid aluminum.

The controversial work of Hansen, Tuset, and Haarberg [50] was criticized by Motzfeldt [51] and Kaptay [52]. Motzfeldt suggested that the reactions between sodium and sapphire crucible (Al_2O_3) may have caused the odd results of Hansen. Kaptay considered the reactions between Al(g) and NaF(s) to exist in Hansen's EMF experiments based on his thermodynamic calculations. But Hansen, Tuset, and Haarberg [53, 54] stood by their results.

To further investigate this issue, Fellner, Korenko, and Danielik [55] carried out experiments at temperatures of 1023 and 1233 K by depositing sodium into molten aluminum cathode by the electrolysis of the molten mixture of 26.4% NaF+73.6% NaCl. Their results did not confirm the high values of sodium solubility in liquid aluminum published by Hansen, Tuset, and Haarberg [50]. Further, Fellner et al. [56] achieved saturated solubility of sodium in liquid aluminum at 983, 1023, 1073, 1173 and 1233 K using the same method. Their results are close to the previous results [46, 48, 49].

Hansen is currently conducting new experiments [57]. In his new experimental process, he has realized that his EMF results were caused by a side-reaction between sodium and sapphire and that the true solubility of sodium in liquid aluminum is close to that determined by the previous studies [46, 48, 49]. The results from his quenching experiment might have been caused by sodium inclusion [57].

All thermochemical investigations on the Al-Na system concentrated on measuring the activity and activity coefficient of sodium in aluminum. Mitchell and Samis [58] determined the distribution of sodium by quenching samples and subsequent chemical analysis. They found that

the activity coefficient of sodium strongly increases with the sodium content between 0 and 85ppm. Dewing [59] determined the sodium content of aluminum in equilibrium with NaF(s) and Na_3AlF_6(s) over a temperature range from 952 to 1149 K by measuring the vapor pressure of sodium over a mixture of aluminum, sodium fluorite, and cryolite by a gas transference method. The activity coefficient of sodium in liquid aluminum was expressed as follows:

$$\frac{RT \ln \gamma_{Na}}{n_{Al}^2} = 8290 + 3.73T,$$ (23)

where γ_{Na} is the Henry's activity coefficient of sodium and n_{Al} is the molarity of liquid aluminum.

Later, Dewing [60] measured the sodium content in liquid aluminum in contact with NaF-AlF3 melts at 1293 and 1353 K using the same method. Brisley and Fray [61] determined the sodium activity in molten super-purity aluminum (at. % aluminum = 99.99), commercial-purity aluminum (at. % aluminum = 99.41), and aluminum alloys LM6 using a sodium β-alumina electrolyte at 998 K. They found that sodium in liquid super-purity aluminum obeys Henry's law between 1 and 50ppm with, $\gamma_{Na} = 222 \sim 355$ which is in agreement with the value obtained by Dewing [60] and Ransley and Neufeld [49]. Yao and Fray [62] investigated the activity of sodium in liquid aluminum with 0.5% impurities using a sodium probe based on Nasicon ($Na_3Zr_2Si_2$-PO_{12}) and air-sintered $Na_{0.75}CoO_2$ solid solution electrode at 1023, 1068, and 1098 K. They found that the activity coefficient of sodium strongly depends on the sodium concentration near the melting point of aluminum and that Henry's law is obeyed at higher temperatures. Sun and Yang [63], who also used sodium β-alumina sensors, measured the activities of sodium in liquid aluminum with 0.11% silicon at 1000 K and found γ_{Na} increases from 0.16 to 22 with increasing the sodium concentration from 1 to 150 ppm. Henry's law was obeyed when the sodium contents were less than 0.04 % in the liquid aluminum. Dubreuil and Pelton [64] measured the potentials of a sodium β-alumina sensor immersed in liquid aluminum with 1 to 100 ppm sodium at 983 to 1023 K. Hansen, Tuset, and Haarberg [50] measured the activity data on sodium in liquid Al-Na alloys by a coulometric titration technique using a galvanic cell employing CaF_2 as a solid electrolyte at 1023, 1073, and 1123 K. They found that the activities exhibit strong negative deviation from Henry's law. This behavior was explained by formation of sodium clusters in the liquid. Their results are not used in this work because of the errors discussed above.

Given that the solubility of sodium in aluminum is fairly low and activities of sodium in liquid aluminum are very sensitive to the purity of aluminum, only partial works of Brisley and Fray [61] in molten super-purity aluminum (at. % aluminum = 99.99) and Dewing [60] were used in the evaluation of model parameters in the present work.

Based on the experimental data in earlier studies [46, 48, 49], Murray [47] determined the thermodynamic model parameters of the Al-Na system. The liquid was treated as a regular solution with excess entropy, and the fcc phase was treated as a Henrian solution. The assessment results resulted in good agreement with the solubility of sodium in liquid aluminum available at that time. However, thermochemical experimental data were not considered.

6.1.2   Ca-Na System

The Ca-Na system was first studied by Metzger [65], who observed an upper and a lower layer in a solidified alloy. Because of the difficulty of separating the two immiscible liquid phases, Lorenz and Winzer [66, 67] and Rinck [68] used the reaction $Ca + 2NaCl = CaCl_2 + 2Na$ at various temperatures to indirectly determine the miscibility gap. At the same time, they investigated the liquidus and monotectic reaction using thermal analysis. However, Lorenz and Winzer [66, 67] reported an incorrect melting temperature of pure calcium as a result of nitride contamination, while the value of Rinck [68] is more reliable. No thermochemical data have been reported in the literature.

Based on the experimental data of Rinck [68], Pelton [69] evaluated the thermodynamic model parameters of the Ca-Na system. The calculated Ca-Na phase diagram reproduced the experimental data in the liquid miscibility gap very well, but no mutual solubilities were assumed between the solid calcium and sodium phases.

6.1.3   K-Na System

The K-Na binary system was investigated several times using the freezing-point method [70-75]. In these works, the liquidus as well as temperatures and compositions of the eutectic and peritectic reactions were established, and the intermetallic compound KNa_2 was identified. However, the solubilities of the bcc phases in one another were indicated to be zero. Moreover, their results lacked accuracy without chemicals of high purity, inert atmosphere protection, and thermometry with high accuracy [76].

Further studies were carried out by MacDonald, Pearson, and Towle [77] using electrical resistance measurements and by Rimai and Bloembergen [78] using nuclear magnetic resonance. Their results showed the existence of bcc solid solution.

Ott et al. [76] investigated the K-Na phase diagram using a freezing-point apparatus and a cryogenic calorimeter. The melting points of the pure metals, the liquidus, and the limits of solubility in the solution regions were determined with a high precision (±0.1 K). No intermetallic compounds other than KNa_2 were found. The temperature and compositions for the eutectic and peritectic reactions were obtained as 260.53 K, 31.9 at. % sodium and 280.07 K, 59.8 at. % sodium, respectively.

The crystal structure of KNa_2 was determined by Laves and Wallbaum [40] using x-ray diffraction. Krier, Craig, and Wallace [79] measured the isobaric heat capacity of KNa_2 between 12 and 320 K and the temperature of the eutectic point and the incongruent melting point of KNa_2 using calorimetry. The formation enthalpy of KNa_2 was estimated to be −1802.04 J/mol at 280 K by Hultgren et al. [39].

The enthalpy of mixing in the liquid was measured by Joannis [70], Bichowsky and Rossini [80], Kawakami [81], and McKisson and Bromley [82] using rough calorimetric measurements. Their results are not used in this work because of poor accuracy and the large scatters in their results. Yokokawa and Kleppa [83] determined the enthalpy of liquid mixing at 384 ± 2 K with accurate reaction calorimetry. Their results are used in the present work.

The literature is rich with experimental data on the activities of sodium and potassium in liquid. The activities of sodium and potassium in the liquid at 384 K were investigated by Cafasso, Khanna, and Feder [84] using vapor-phase absorption spectrophotometry of atomic resonance lines. Kagan [85] measured the activities of potassium in the liquid at 400 K using an effusion method. Lokshin and Ignatov [86] investigated the activity of potassium in liquid using EMF at 520 K. The investigations of the above authors indicate that activities of sodium and potassium show positive deviation from Raoult's law. Lantratov [87] measured the activity of potassium in liquid using EMF at 723 and 773 K. However, Lantratov's results, which are not used in the present work, are unreliable because of the reaction between molten alkali metals and silicic acid glass, which was used as an elecyrolyte in the experiments [88]. All activity data are later compared with calculated values.

6.1.4   Li-Na System

The Li-Na system has been investigated many times using different techniques, especially in the vicinity of the consolute point. The miscibility gap was investigated by Schurmann and Parks [89]; Feistma et al. [90]; Down, Hubberstey, and Pulman [91, 92]; and Endo et al. [93] using the electrical resistivity measurement technique; by Kandan, Faxon, and Keller [94] using the density measurement technique; and by Wu and Brumberger [95] using light microscopy, X-ray, and neutron-scattering techniques. As shown in the Table 6.1, their results were very close to each other. No thermochemical data have been reported in the literature.

Bale [96] reviewed available experimental data in the literature and made a qualitative thermodynamic analysis of the system assuming zero solubility in the bcc phases. The phase boundary of the liquid miscibility gap was represented by an analytical function of the temperature and the mole fraction of sodium based on the experimental data summarized by Feistma et al. [90]. Pelton [97] further thermodynamically modeled the liquid phase of the system based on Bale's review [96]. The solid solubility values at the monotectic and eutectic temperatures were estimated by applying Raoult's law. However, the calculated phase diagram differs from experimental data near the consolute point of the miscibility gap (see Fig. 6.5). Furthermore, no model parameters of solid solution phases were given.

6.1.5   Mg-Na System

Mathewson [45] determined the solubility of sodium in liquid magnesium as 2 at. % at the monotectic temperature of 911 K by thermal analysis. An almost identical value was found by Lantratov [87]—2.1 at. % and 911 K. However, both of these researchers used glass containers, which usually react with sodium and magnesium and affect the results. Klemm and Kunze [98] used an iron crucible and measured the solubility of magnesium in liquid sodium by weight-loss and chemical-analysis techniques. No intermetallic phases were detected by X-ray investigations in this binary system.

Lantratov [87] measured the activities of sodium and magnesium in liquid using the EMF method at 973 K over the entire concentration range. The activities of sodium and magnesium exhibit very large positive deviation from Raoult's law as a result of phase separation. Rosenkilde, Arnesen, and Wallevik [7] measured the concentration of sodium in liquid magnesium in equilibrium with $NaCl$-$MgCl_2$ melts of different compositions and temperatures from 923 to 1063 K at very low sodium concentrations.

Based on the experimental data in the literature [87, 98], Pelton [99] made a qualitative thermodynamic analysis of the Mg-Na system and used the van't Hoff equation to analyze the liquid miscibility gap. No models or thermochemical data were considered.

6.2   Ternary Systems

Because of the lack of experimental data in all the ternary systems, the thermodynamic description of the ternary systems was predicted by combining the thermodynamic description of the corresponding three sub-binary systems. The Ca-Li-Na ternary system was investigated to study the characteristics of the ternary liquid miscibility gap. The Al-Mg-Na ternary system was investigated to further study the effect of sodium on high-temperature embrittlement of Al-Mg alloys.

6.3   Model Parameter Evaluation

All model parameters were evaluated using the Parrot module in Thermo-Calc [100]. This program is able to accept various kinds of experimental data in one operation. It works by minimizing an error of sum, with each of the selected data given a certain weight. The weight was chosen and adjusted based on the data uncertainties given in the original publications and on the authors' judgment by examining all experimental data simultaneously. All thermodynamic calculations were carried out using Thermo-Calc.

The complete and self-consistent thermodynamic descriptions for the Al-Na, Ca-Na, K-Na, Li-Na, and Mg-Na binary systems thus obtained are listed in Table 6.1. The reference state of the Gibbs energy of individual phases is the so-called SER state (i.e., the enthalpies of the pure elements in their stable states at 298.15 K and 1 bar).

The parameter evaluation procedure in the Al-Na system started with the miscibility gap in the liquid phase with the selected experimental data on the solubility of sodium in liquid aluminum and the activities of sodium in liquid aluminum. The thermodynamic parameters of the fcc and bcc phases were then evaluated. Given there is an hcp phase in the Mg-Na binary system, the thermodynamic parameter of the metastable hcp phase was set to a large positive value so it did not become stable in the system. Many iterations were necessary to reproduce all experimental data. Finally, the model parameters of all phases were simultaneously adjusted with all experimental data included.

In the Ca-Na system, the parameters of the liquid phase were taken from Pelton [69]. The thermodynamic parameters of the bcc phase were evaluated using the experimental liquid boundary data and the monotectic temperature and composition of the liquid phase. The parameters of the fcc phase were arbitrary because of the lack of data. The thermodynamic parameter of the metastable hcp phase, which will be present when magnesium is added in future work, was set to an arbitrary positive value so it did not become stable in the system.

The evaluation of model parameters in the K-Na system started with the liquid phase, followed by the bcc-phase miscibility gap and the intermetallic compound KNa_2 using the experimental-phase boundary data and thermodynamic data. Because the experimental data by Ott et al. [76] are more reliable than others [70-75, 77, 78], more weight was given to the former data than the

latter. In the evaluation process, the enthalpies of mixing in bcc from first-principles calculations were considered as experimental data. Finally, all the model parameters were refined by simultaneous optimization of all the experimental and first-principles data.

The evaluation of model parameters in the Li-Na system started with the liquid miscibility gap followed by the bcc-phase miscibility gap. Special attention was paid to the composition and temperature of the consolute point in the liquid miscibility gap to ensure the rational shape of the miscibility gap because it was not well reproduced by Pelton [97]. The thermodynamic parameters of the metastable fcc and hcp phases were set to an arbitrary positive value so they did not become stable in system. The miscibility gap in the liquid phase requires a positive $^{o}L^{liq}_{Li,Na}$. The consolute point of the liquid miscibility gap is lithium-rich; therefore, parameter $^{1}L^{liq}_{Li,Na}$ is positive. The parameter $^{2}L^{liq}_{Li,Na}$ and the temperature dependence of the parameter $^{o}L^{liq}_{Li,Na}$ are added to better reproduce the phase-equilibrium data. The parameter $^{o}L^{bcc}_{Li,Na}$ is also positive because of the miscibility gap in the bcc phase.

The evaluation procedure in the Mg-Na system started with the liquid miscibility gap, followed by the bcc and hcp phases. The activities of sodium in liquid magnesium were used at the same time. Given there is an fcc phase in the Mg-Na binary system, the thermodynamic parameters of the metastable fcc phase were set to a large positive value so they did not become stable in the system. Finally, the model parameters of all phases were simultaneously adjusted with all experimental data included.

6.4 Results and Discussions

6.4.1 Al-Na System

The calculated phase diagram using the present thermodynamic description of the Al-Na system is shown in Fig. 6.1. A much more positive interaction parameter in the liquid phase than that of Murray [47], $^{0}L^{Liq}_{Al,Na}$, has been obtained in the present work because the most recent data show lower solubility of sodium in liquid aluminum, as reported in the literature [56] (see Fig. 6.2).

Fig. 6.2 gives the enlarged view of the Al-rich part of the calculated phase diagram in comparison with previous work by Murray [47] (dashed lines) and all the available experimental data. The relative standard deviations, calculated using the formula in Eq. (24) below, are included in each figure caption.

$$\sigma = \sqrt{\frac{1}{n}\sum_{i=1}^{n}\left(\frac{x_i^{cal} - x_i^{\exp}}{x_i^{\exp}}\right)^2} , \qquad (24)$$

where x_i^{cal} is the calculated result, $x_i^{\exp}$ is the experimental datum, and n is the number of experimental data. The calculation reveals that the calculated phase diagram shows an excellent agreement with all the experimental data, especially the recent results. However, the work by Murray [47] fits only part of the experimental data and does not agree with the most recent data by Fellner et al. [56]. The invariant reactions in Al-Na system are listed with the experimental data included and show good agreement. Fig.6.3 shows the calculated activities of sodium in

liquid aluminum at 998, 1293, and 1353 K, respectively, in comparison with experimental data. It shows that the activities of sodium in liquid have a large temperature dependence. The calculated values do not fit the experimental data very well at 1353 K, at which point the concentration of sodium is beyond 0.03 at. %. Dewing [101] pointed out that quenching might well have been inadequate in these experimental data.

6.4.2 Ca-Na System

The phase diagram calculated using these parameters is shown in Fig. 6.4, with the experimental data superimposed. It shows that the most of the experimental liquidus data are well reproduced. The invariant reactions in the Ca-Na system listed in Table 6.2 are identical to the experimental data.

6.4.3 Li-Na System

Fig. 6.5 shows the calculated phase diagram using the present thermodynamic description in comparison with that of Pelton [97] and experimental data. It is seen that the present calculation better reproduces the experimental data. The invariant equilibriums and consolute point in Li-Na system are listed in Table 6.2 along with the experimental data.

6.4.4 K-Na System

The calculated K-Na phase diagram is shown in Fig. 6.6, with the experimental data superimposed. Fig. 6.7 and 6.8 depict the activities in the liquid and the calculated enthalpy of mixing in the liquid, respectively, compared to the experimental data. The calculated enthalpy of mixing in the bcc phase at 298 K is shown in Fig. 6.9 in comparison with the results from first-principles calculations. The calculated temperatures and compositions of the invariant reactions are listed in Table 6.2 along with the experimental data.

6.4.5 Mg-Na System

The calculated phase diagram using the present thermodynamic description is presented in Fig. 6.10 and shows excellent agreement in comparison with the experimental data. Fig.6.11 provides a magnified view of the sodium-rich part of the calculated phase diagram. The invariant equilibrium in the Mg-Na system is listed in Table 6.2 along with the experimental data. As shown in this table, very good agreement is obtained. Fig. 6.12 shows the calculated activity of sodium and magnesium in liquid at 973 K along with the experimental data. Good agreement has been obtained except for the activity of sodium in the liquid miscibility gap, in which the experimental data are almost equal to unity and seem unreasonable.

6.4.6 Ca-Li System

The Ca-Li system was modeled by Grobner et al. [43] carefully. Their results are in good agreement with experimental data and are accepted in the present work. The calculated phase diagram is shown in Fig. 6.13.

6.4.7　Al-Mg System

The Al-Mg system was modeled by Liang et al. [42] carefully. Their results are in good agreement with experimental data and are accepted in the present work. The calculated phase diagram is shown in Fig.6.14.

6.4.8　Ca-Li-Na System

The calculated liquidus projection of the Ca-Li-Na ternary system is presented in Fig. 6.15, and the primary phases forming from the liquid phase during solidification are shown. The dotted lines are isotherms, with the numbers indicating the temperature in degree Kelvin. The figure shows that the liquid miscibility gap at high temperatures in the Ca-Na system smoothly connects to the liquid miscibility gap at low temperatures in the Li-Na system. Fig. 6.16, 6.17, and 6.18 show the liquidus projection of the sodium-rich corner. This corner is complex because of several narrow phase regions. The invariant equilibriums in the liquidus projection are listed in Table 6.3. As a result of the liquid miscibility gap, the invariant reactions involving both liquid phases appear twice on the liquidus projection. Although they have the same temperatures, the same compositions, and the same phases, as shown in Table 6.3, the reaction types and the directions are different [93].

Fig. 6.19 and 6.20 show the calculated isothermal sections at 900 and 510 K. The former shows the shape of the liquid miscibility gap, while the latter shows the binary compound CaLi$_2$ region. Fig. 6.21, 6.22, and 6.23 show the calculated isopleth sections of the Ca-Li-Na system at the condition of $x_{Ca} = x_{Li}$, $x_{Ca} = x_{Na}$, and $x_{Li} = x_{Na}$, respectively. The calculations in the ternary system are complex because of the miscibility gaps involving three bcc phases and two liquid phases [100].

6.5　Summary

The binary Al-Na, Ca-Na, Li-Na, K-Na, and Mg-Na systems were modeled by computational thermodynamics using the CALPHAD method. Self-consistent thermodynamic parameters of the binary systems were obtained.

Combined with the Ca-Li and Al-Mg system modeling from the literature, the phase equilibriums of the Ca-Li-Na and Al-Mg-Na systems were calculated. Isothermal and isopleth sections of the ternary system and the projection of the liquidus surface have been presented.

This database development paves the way for investigation of the impurity effects on processing of aluminum alloys through understanding phase stability under various processing conditions.

Table 6.1. Thermodynamic parameters of the Al-Na, Ca-Na, Li-Na, K-Na, and Mg-Na systems in standard international units

System	Phase	Model	Parameter	Value (J/mol)
Al-Na	liquid	(Al, Na)	${}^0L_{Al,Na}^{liq}$	773708 + 20.277T
			${}^1L_{Al,Na}^{liq}$	−745869
	bcc	(Al, Na)	${}^0L_{Al,Na}^{bcc}$	20000
	fcc	(Al, Na)	${}^0L_{Al,Na}^{fcc}$	78765
	hcp	(Al, Na)	${}^0L_{Al,Na}^{hcp}$	20000
Ca-Na	liquid	(Ca, Na)	${}^0L_{Ca,Na}^{liq}$	28896 − 8.35T
			${}^1L_{Ca,Na}^{liq}$	−33 − 7.03T
	bcc	(Ca, Na)	${}^0L_{Ca,Na}^{bcc}$	56258 − 39.401T
	fcc	(Ca, Na)	${}^0L_{Ca,Na}^{fcc}$	30000
	hcp	(Ca, Na)	${}^0L_{Ca,Na}^{hcp}$	15000
Li-Na	liquid	(Li, Na)	${}^0L_{Li,Na}^{liq}$	10684
			${}^1L_{Li,Na}^{liq}$	3896 − 5.539T
	bcc	(Li, Na)	${}^2L_{Li,Na}^{liq}$	1580
	fcc	(Li, Na)	${}^0L_{Li,Na}^{bcc}$	16000
	hcp	(Li, Na)	${}^0L_{Li,Na}^{fcc}$	20000
K-Na	liquid	(K, Na)	${}^0L_{K:Na}^{liq}$	2916 − 0.517T
			${}^1L_{K:Na}^{liq}$	−766 + 1.044T
	bcc	(K, Na)	${}^0L_{K:Na}^{bcc}$	11445 − 10.037T
			${}^1L_{K:Na}^{bcc}$	−1595 − 2.336T
	fcc	(K, Na)	${}^0L_{K,Na}^{bcc}$	15000
	hcp	(K, Na)	${}^0L_{K,Na}^{fcc}$	15000
	KNa$_2$	(K)$_1$(Na)$_2$	G^{KNa_2}	${}^oG_K^{bcc} + 2\,{}^oG_{Na}^{bcc} - 1949 + 3.866T$
Mg-Na	liquid	(Mg, Na)	${}^0L_{Mg,Na}^{liq}$	25975
			${}^1L_{Mg,Na}^{liq}$	4370
	bcc	(Mg, Na)	${}^0L_{Mg,Na}^{bcc}$	30000
	fcc	(Mg, Na)	${}^0L_{Mg,Na}^{fcc}$	20000
	hcp	(Mg, Na)	${}^0L_{Mg,Na}^{hcp}$	37566

Table 6.2. Invariant reactions and consolute points in Al-Na, Ca-Na, Li-Na, K-Na, and Mg-Na

System	Reaction	Reference	Temperature (K)	Concentration of Na in at. %		
Al-Na	$gas \rightarrow liquid1 + liquid2$	Present work	1157	100	0.238	100
	$liquid1 \rightarrow fcc(Al) + liquid2$	Present work	932	0.14	0.002	100
		Experiment [45]	930	—	—	—
		Experiment [48]	932	0.18	<0.003	—
		Experiment [49]	932	0.14	0.002	—
	$liquid2 \rightarrow fcc(Al) + bcc(Na)$	Present work	371	99.99	7.03×10^{-0}	100
		Experiment [45]	371	—	—	—
		Present work	1157	100	0.238	100
		Present work	932	0.14	0.002	100
Ca-Na	$liquid1 \rightarrow bcc(Ca) + liquid2$	Present work	983.9	22.1	10.2	95.9
		Experiment [68]	983 ± 10	0.221	—	95.9
	$bcc(Ca) \rightarrow fcc(Ca) + liquid2$	Present work	707.3	0.563	0.363	99.5
	$liquid2 \rightarrow fcc(Ca) + bcc(Na)$	Present work	370.9	99.998	5.180×10^{-3}	99.999
	Consolute point	Present work	1470.3		71.275	
K-Na	$liquid = bcc(Na) + KNa_2$	Present work	280.053	59.3	99.3	66.7
		Experiment [71]	280.03	59.95	—	66.7
		Experiment [73]	280.05	58	—	66.7
		Experiment [74]	280.05	—	—	—
		Experiment [75]	279.75	—	—	—
		Experiment [76]	280.07 ± 0.05	59.8	99.2	66.7
		Experiment [77]	280.5 ± 1	60	97	66.7
		Experiment [79]	280.058 ± 0.001	—	—	—
	$liquid + bcc(K) = KNa_2$	Present work	261.17	30.33	4.3	66.7
		Experiment [71]	260.65	33.36	—	66.7
		Experiment [73]	260.55	—	—	—
		Experiment [75]	260.65	—	—	—
		Experiment [76]	260.53 ± 0.05	31.9	4.6	66.7
		Experiment [77]	261 ± 1	33.4	4.5	66.7
		Experiment [79]	260.51 ± 0.01	—	—	—
Li-Na	$liquid1 \rightarrow bcc(Li) + liquid2$	Present work	444.5	3.4	1.2	90.0
		Experiment [90]	443	3.4	—	90.2
		Experiment [94]	443 + 1	3.4	—	87.87
		Experiment [102]	444	3.4	—	91.6
	$liquid2 \rightarrow bcc(Li) + bcc(Na)$	Present work	360.2	96.5	0.5	99.5
		Experiment [91, 92]	365.3	97.0	—	—
		Experiment [103]	366.5	96.3	—	—
		Experiment [102]	365.4	96.3	—	—
	consolute point	Present work	581.5		33	
		Experiment [89]	577 ± 2		36 ± 2	
		Experiment [90]	576.4		35.7	
		Experiment [91, 92]	578		37	
		Experiment [93]	578		37	
		Experiment [94]	579 ± 1		35	
		Experiment [95]	580		34	
Mg-Na	$gas \rightarrow liquid1 + liquid2$	Present work	1159	84.07	5.93	88.58
	$gas \rightarrow liquid2$	Present work	1157		97.016	
	$liquid1 \rightarrow hcp(Mg) + liquid2$	Present work	910	2.10	0.033	92.70
		Experiment [45]	911	2.0 ± 0.1	—	—
		Experiment [87]	911	2.1	—	98.6
		Experiment [98]	910	1.6	—	92.7
	$liquid2 \rightarrow hcp(Mg) + bcc(Na)$	Present work	371	99.98	4.15×10^{-4}	100.00
		Experiment [45]	371	—	—	—
		Experiment [98]	371	—	—	—

Table 6.3. Invariant reactions in the Ca-Li-Na liquidus projection

| Reaction	Class	Temperature (K)	Composition of Li and Ca in at. %							
			Phase 1		Phase 2		Phase 3		Phase 4	
$liquid1 + + liquid2 + bcc(Ca) \rightarrow fcc(Ca)$	III_1	648.4	40.843	55.467	3.553	2.915	7.767	0.919	5.960	0.938
$liquid2 + bcc(Ca) \rightarrow fcc(Ca) + liquid1$	II_1	648.4	3.553	2.915	7.767	0.919	5.960	0.938	40.843	55.467
$liquid1 \rightarrow fcc(Ca) + CaLi_2 + liquid2$	I_1	503.3	56.827	41.870	9.418	90.507	66.667	33.333	3.853	0.0346
$liquid2 + liquid1 \rightarrow fcc(Ca) + CaLi_2$	II_2	503.3	3.853	0.0346	56.827	41.870	9.418	90.507	66.667	33.333
$liquid1 \rightarrow bcc(Li) + CaLi_2 + liquid2$	I_2	415.0	92.035	6.343	98.335	1.401	66.667	33.333	7.090	6.270×10^{-4}
$liquid2 + liquid1 \rightarrow bcc(Li) + CaLi_2$	II_3	415.0	7.090	6.270×10^{-4}	92.035	6.343	98.335	1.401	66.667	33.333
$liquid2 + fcc(Ca) \rightarrow bcc(Na) + CaLi_2$	II_4	368.5	0.689	6.932×10^{-4}	2.658	97.337	0.121	9.946×10^{-5}	66.667	33.333
$liquid2 + CaLi_2 \rightarrow bcc(Na) + bcc(Li)$	II_5	359.7	3.525	3.720×10^{-5}	66.667	33.333	0.496	3.053×10^{-6}	50.054	8.722×10^{-3}
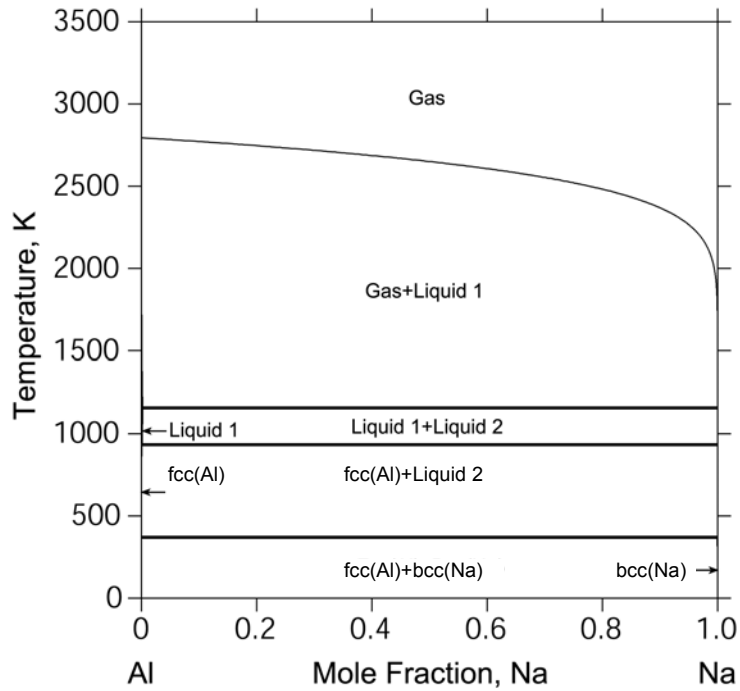
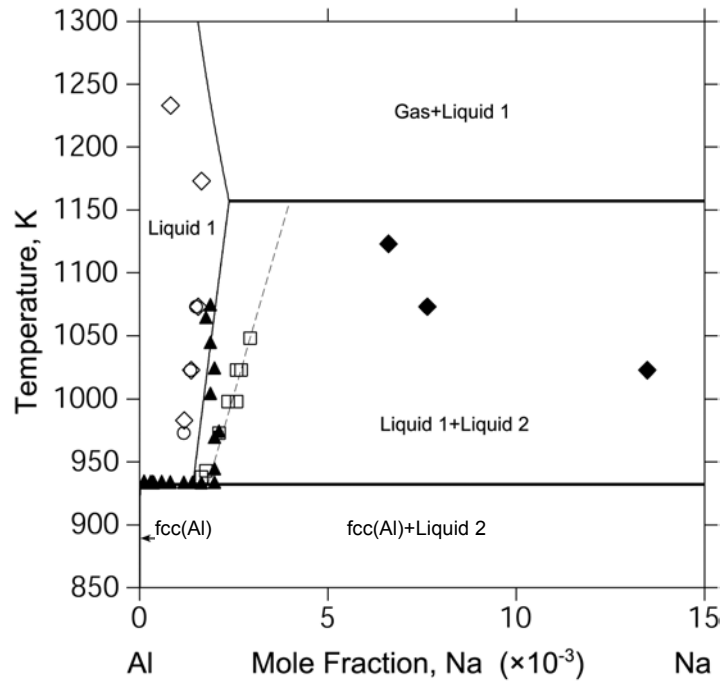**Fig. 6.1. Calculated Al-Na phase diagram.**

Fig. 6.2. Enlarged view of Fig. 6.1 at the aluminum-rich side in comparison with previous work by Murray [47] (dashed lines) and the experimental data ○ by Scheuer [46]; ▲ by Fink, Willey, and Stumpf [48]; □ by Ransley and Neufeld. [49]; ◆ by Hansen, Tusset, and Haarberg [50]; and   by Fellner et al. [56] (σ = 8.67%).

28
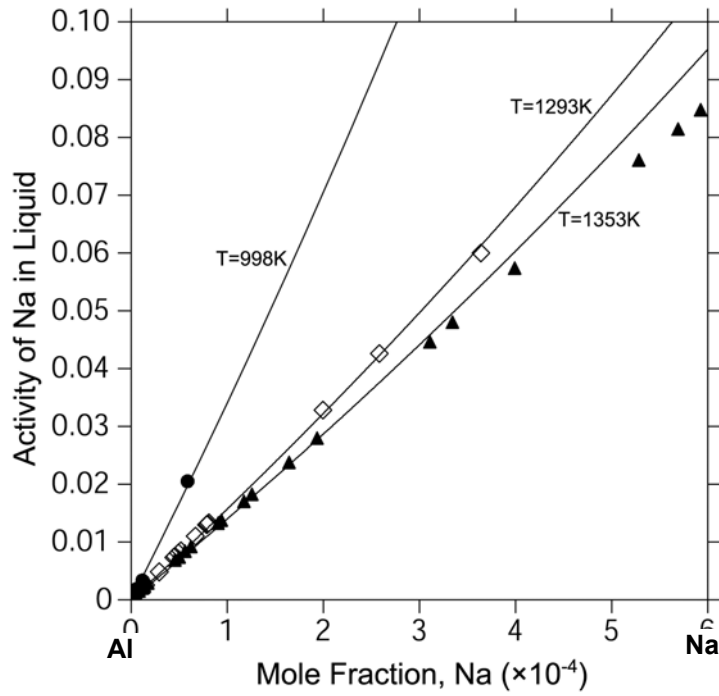
Fig. 6.3. Calculated activity of sodium in liquid in comparison with the experimental data ◇ at 1293 K and ▲ at 1353 K by Dewing [60] and ● at 998 K by Brisley and Fray [61] (σ = 5.42%).
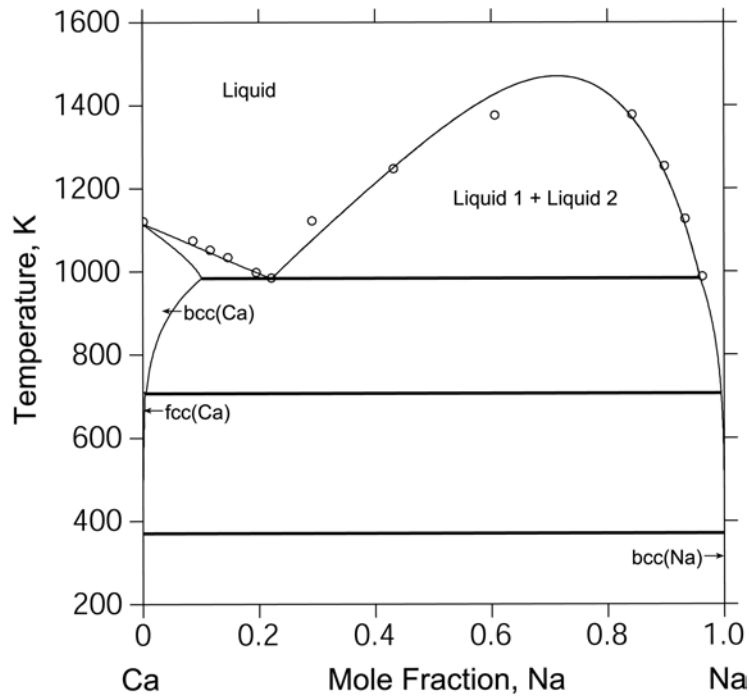

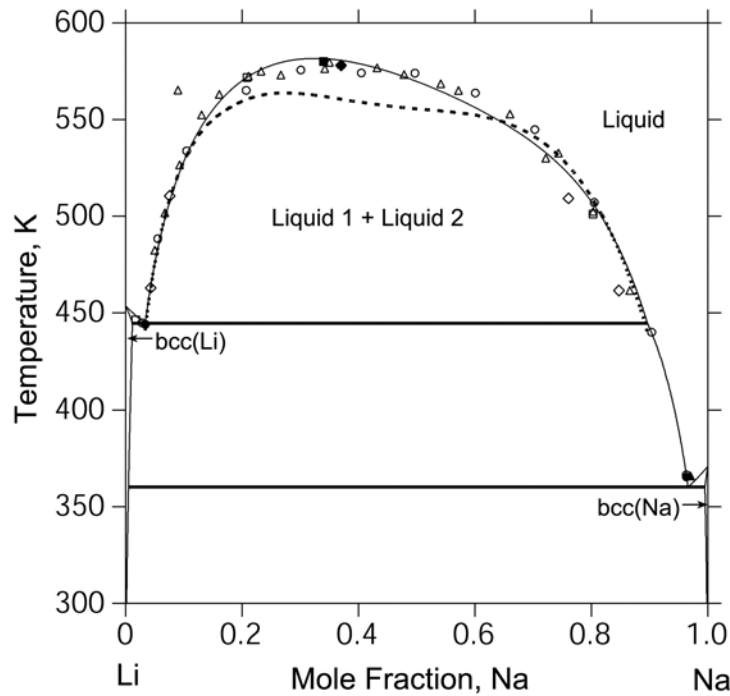**Fig. 6.4. Calculated Ca-Na phase diagram in comparison with the experimental data ○ by Rinck [68].**

Fig. 6.5. Calculated Li-Na phase diagram in comparison with previous work by Pelton [97] (dashed lines) and the experimental data □ [89], ◊ [90], ▲ [91, 92], ◆[93], △ [94], ■[95], ●[102], and ○ [103].
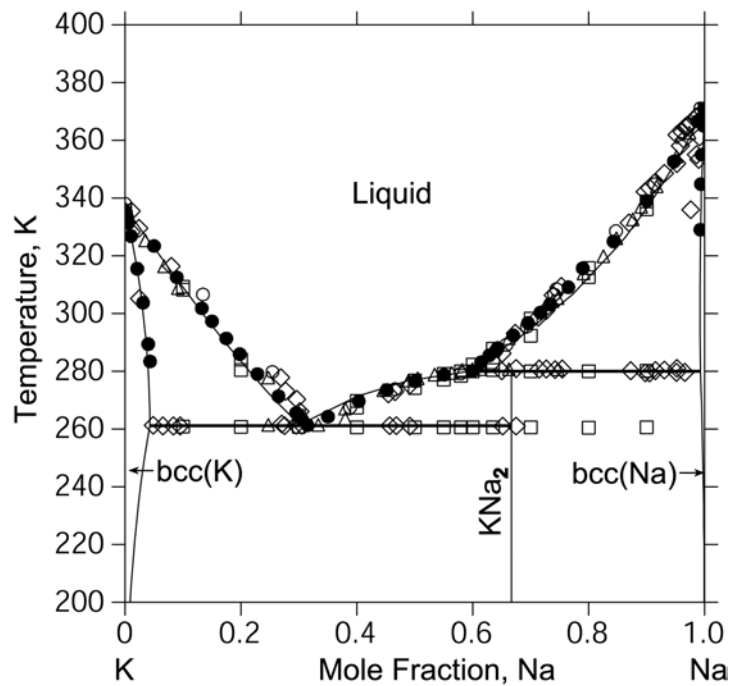
**Fig. 6.6. Calculated K-Na phase diagram in comparison with the experimental data △ [71],□ [73],○ [75], ●
[76], and ◇ [77] (σ = 3.71%).**

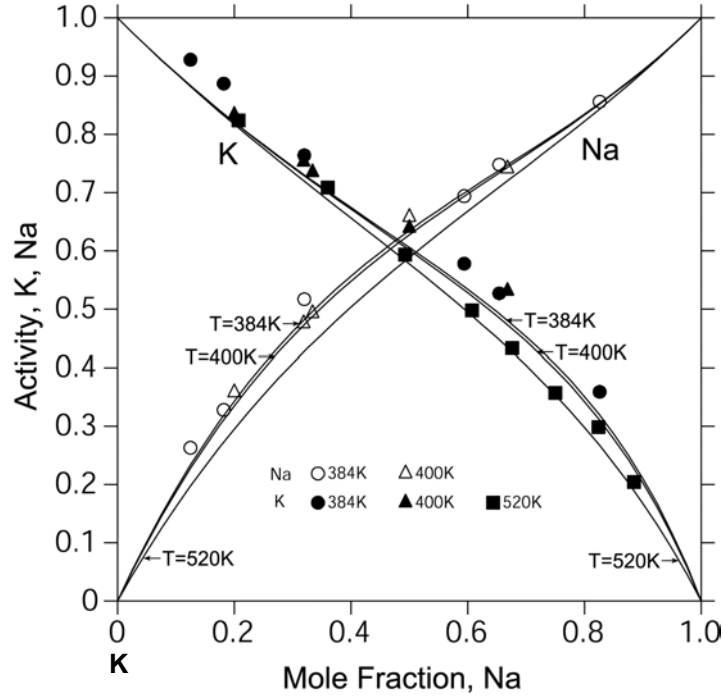**Fig. 6.7. Calculated activity of potassium and sodium in liquid in comparison with the experimental data ○ ● [84], △ ▲[85], and ■[86] (σ = 9.28%).**
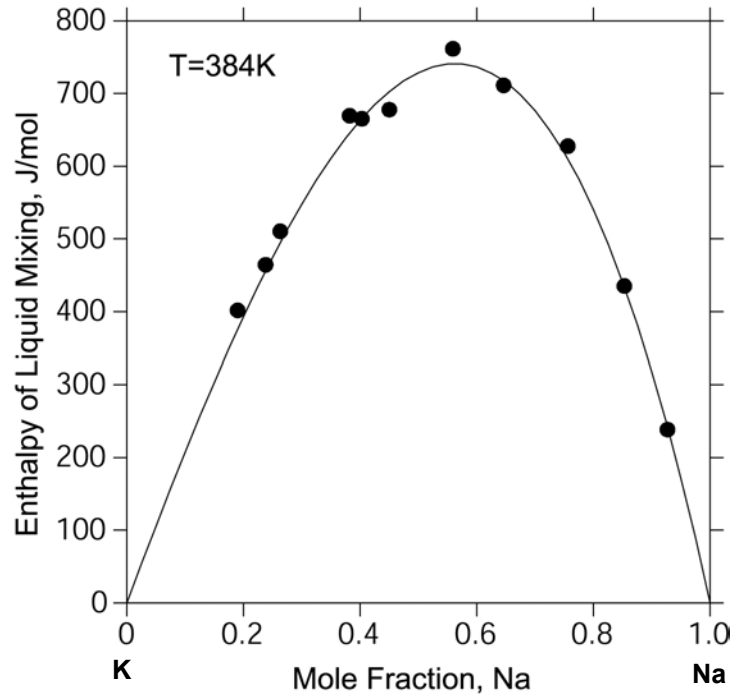
Fig. 6.8. Calculated enthalpy of mixing in the liquid phase at 384 K in comparison with the experimental data ●[83] (σ = 4.43%).
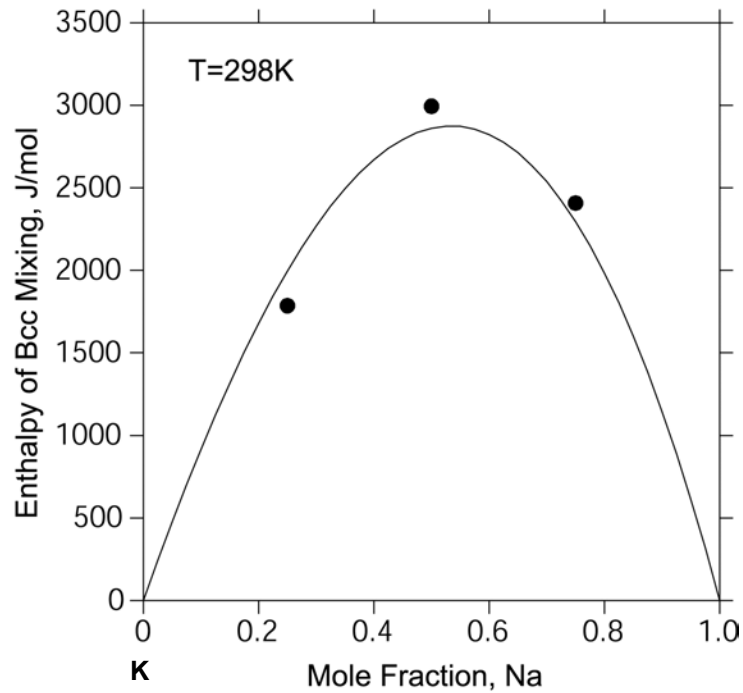
Fig. 6.9. Calculated enthalpy of mixing in the bcc phase at 298 K in comparison with the results from first-principles calculations ● (σ = 7.75%).
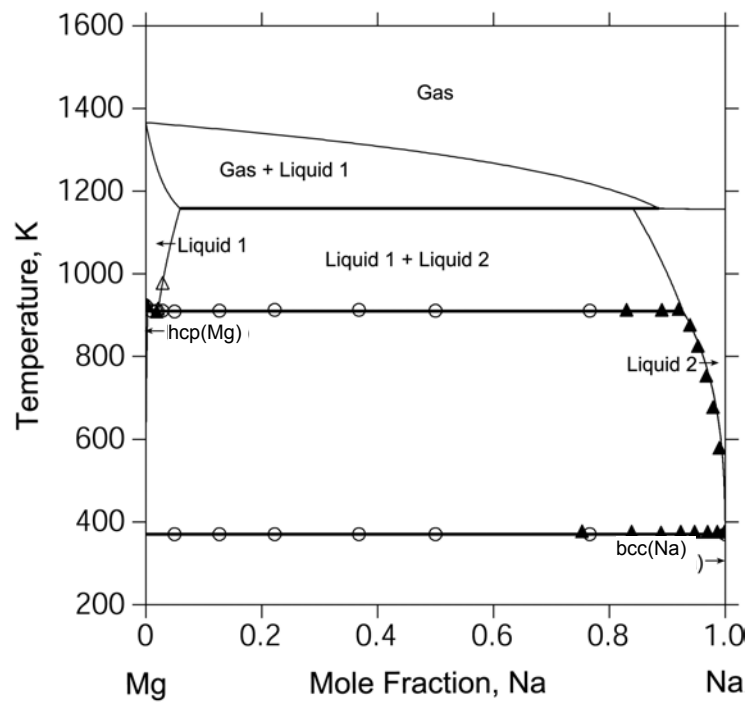
Fig. 6.10. Calculated Mg-Na phase diagram in comparison with the experimental data ○ by Mathewson [45], △ by Lantratov [87], and ▲ by Klemm and Kunze [98] (σ = 1.32%).
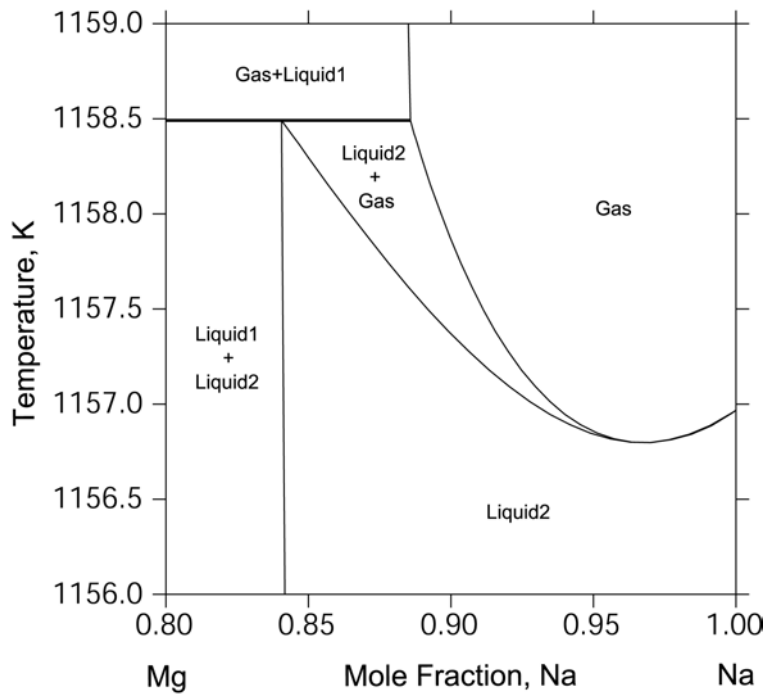
Fig. 6.11. Magnified view of Fig. 6.10 at the sodium-rich side in the Mg-Na system.
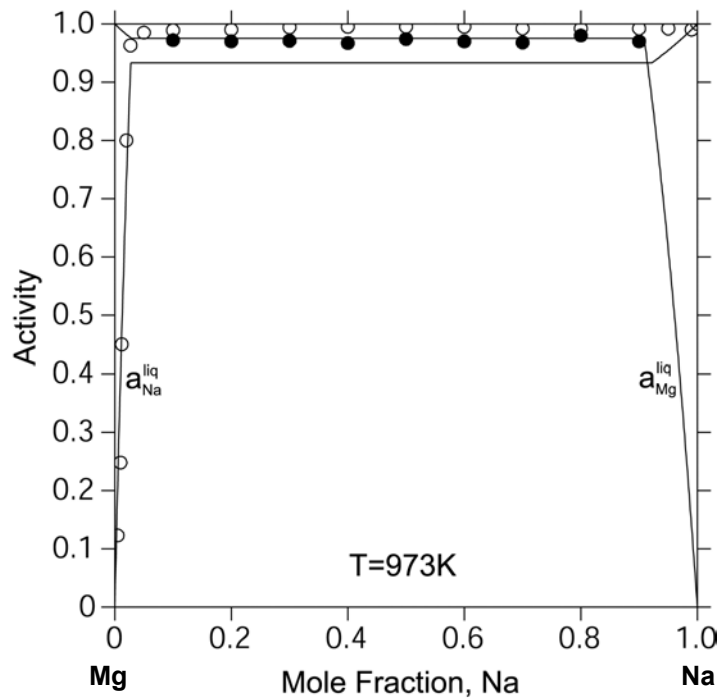
Fig. 6.12. Calculated activities of sodium and magnesium in liquid at 973 K in comparison with the experimental data ○ (a_{Na}^{liq}) and ● (a_{Mg}^{liq}) by Lantratov [87] (σ = 10.5%).

33
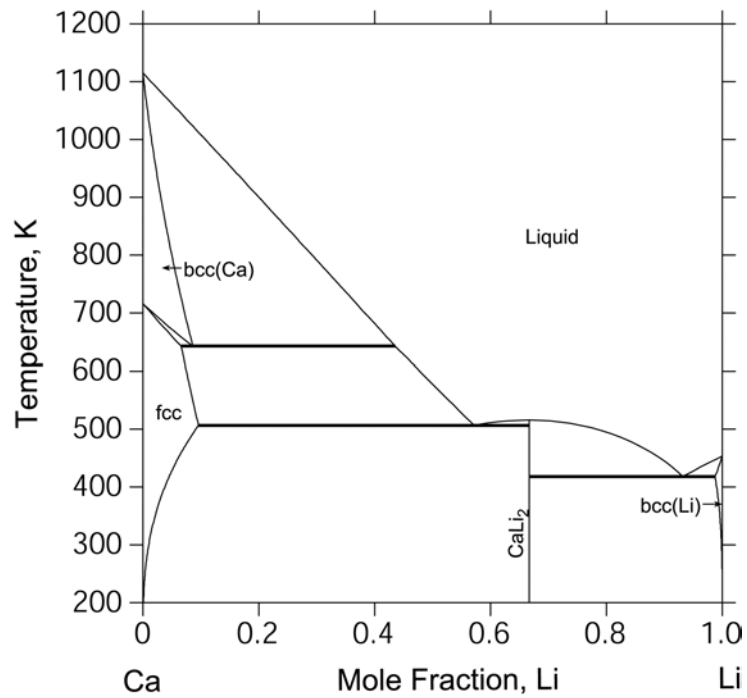
Fig. 6.13. Calculated Ca-Li phase diagram using the thermodynamic parameters by Grobner et al. [43].
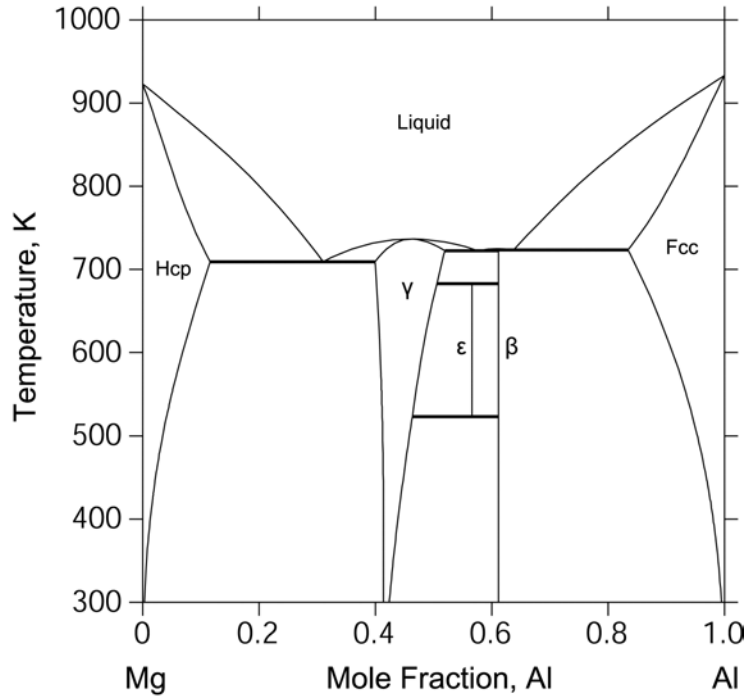
Fig. 6.14. Calculated Al-Mg phase diagram [42].

34
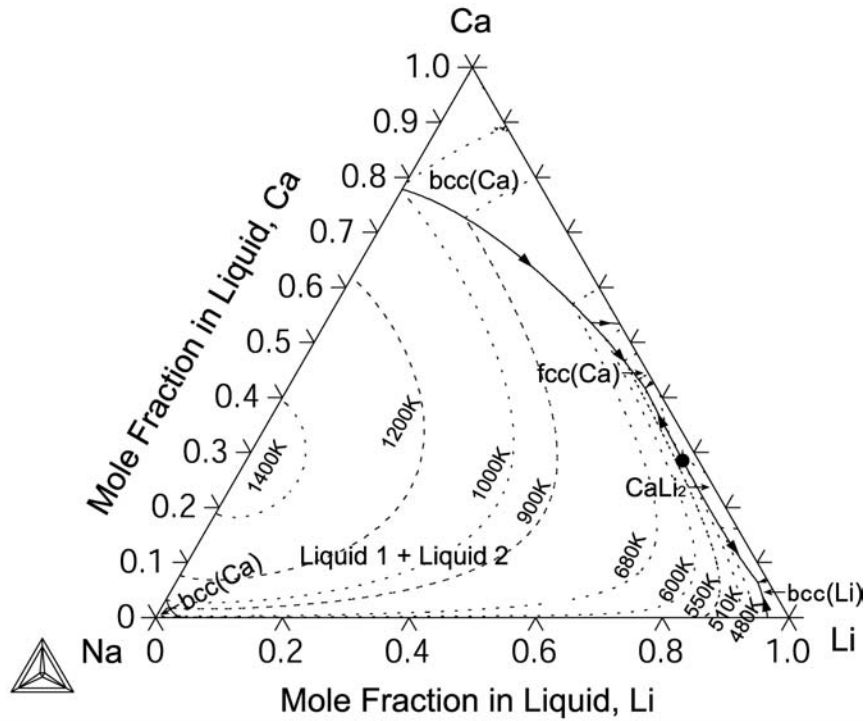
Fig. 6.15. Liquidus projection to the composition triangle in the Ca-Li-Na system with isotherms (dotted lines) superimposed along with their temperatures.
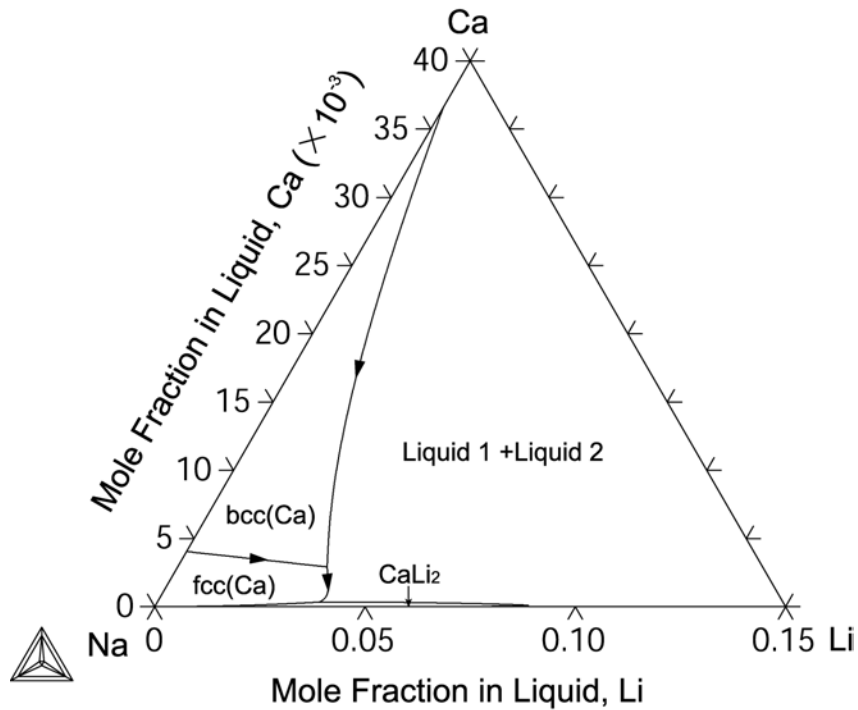
Fig. 6.16. Sodium-rich corner of the liquidus projection with very low mole fractions of Ca on the y-axis.

35
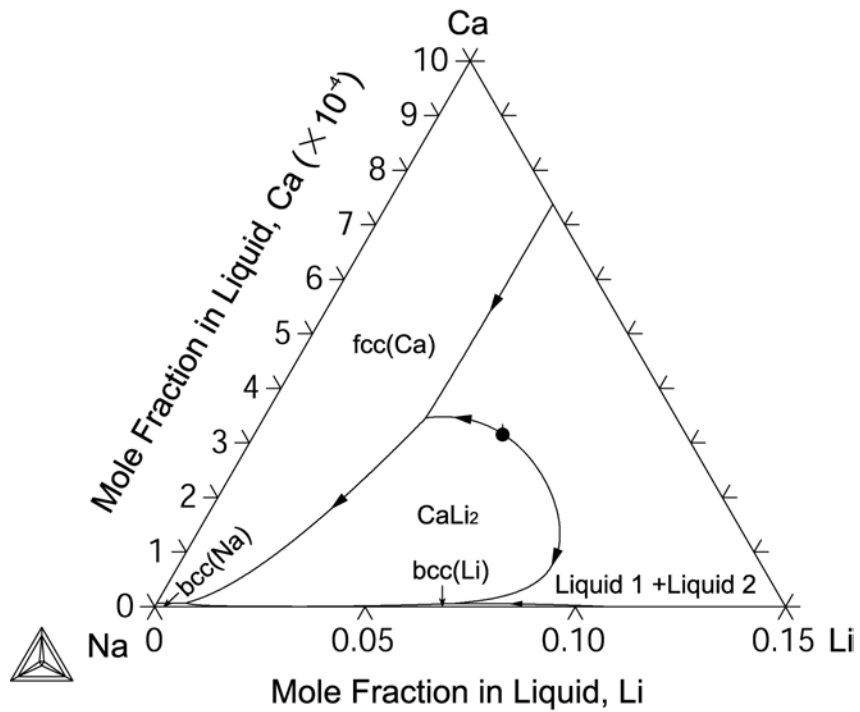
Fig. 6.17. Sodium-rich corner of the liquidus projection with one order lower mole fractions of Ca on the y-axis than that in Fig. 6.16.
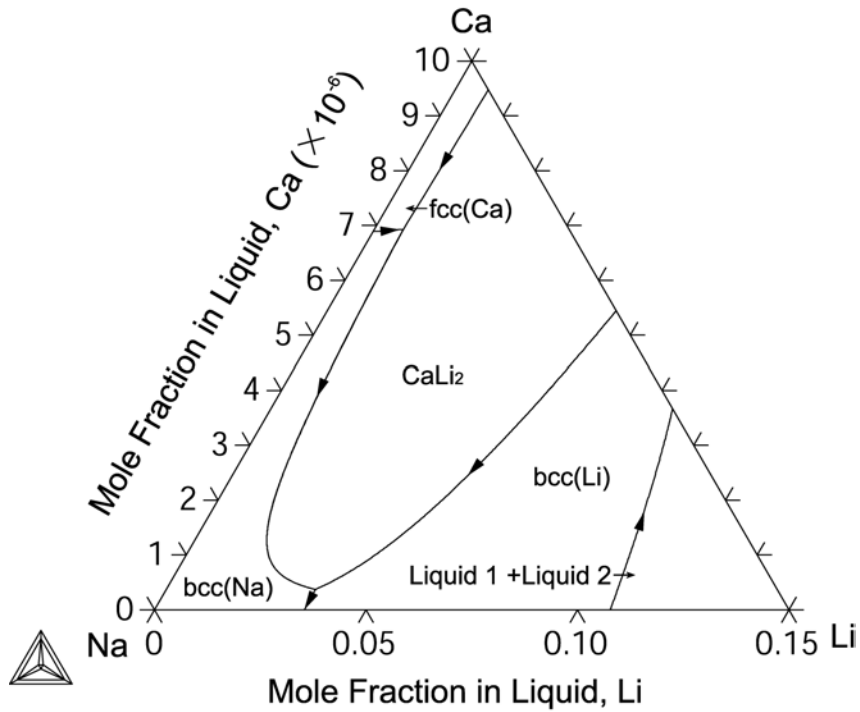
Fig. 6.18. Sodium-rich corner of the liquidus projection with three order lower mole fractions of Ca on the y-axis than that in Fig. 6.16.

36
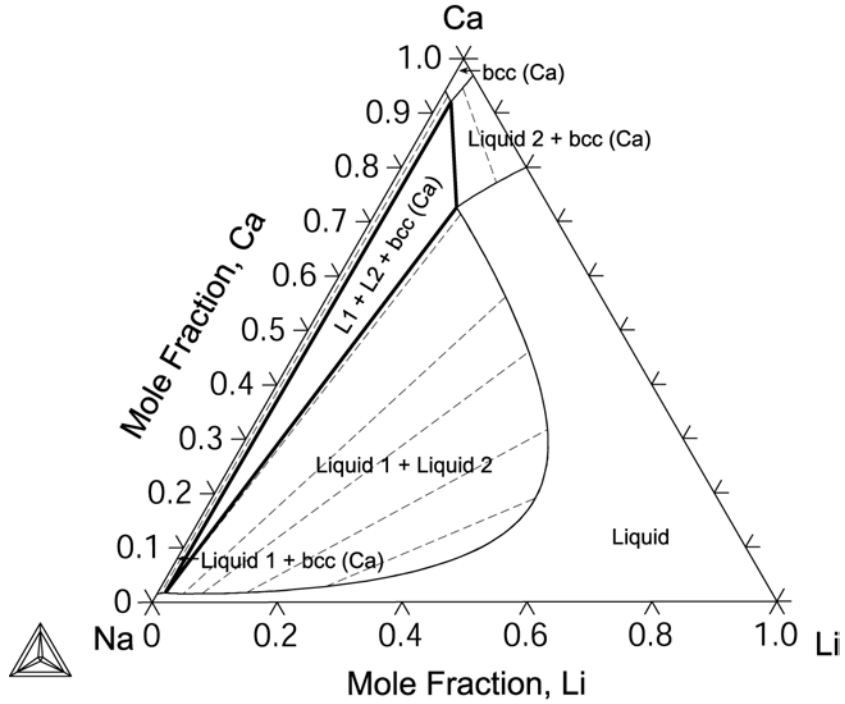
Fig. 6.19. Calculated isothermal section of the Ca-Li-Na system at 900 K.
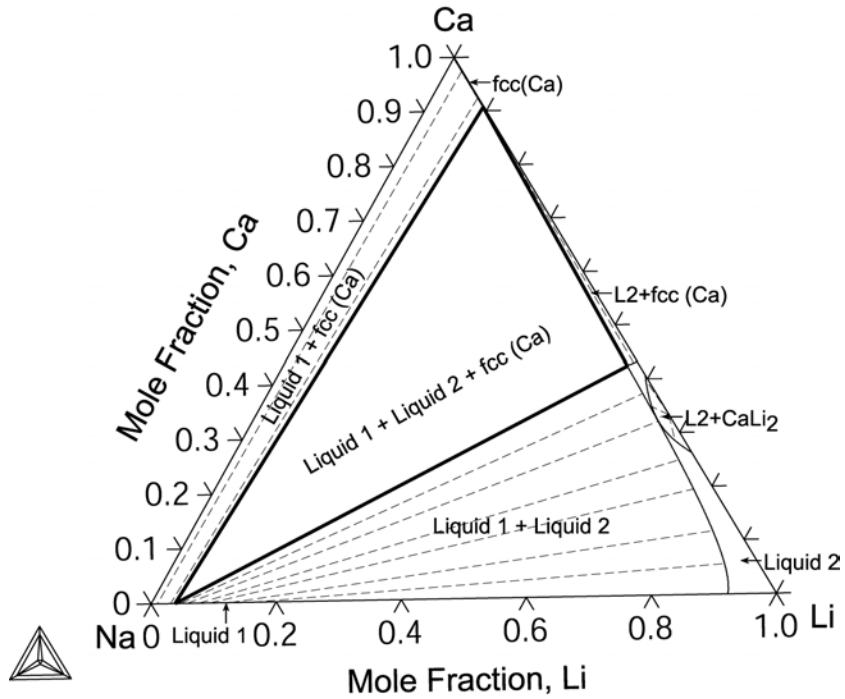
Fig. 6.20. Calculated isothermal section of the Ca-Li-Na system at 510 K.

37
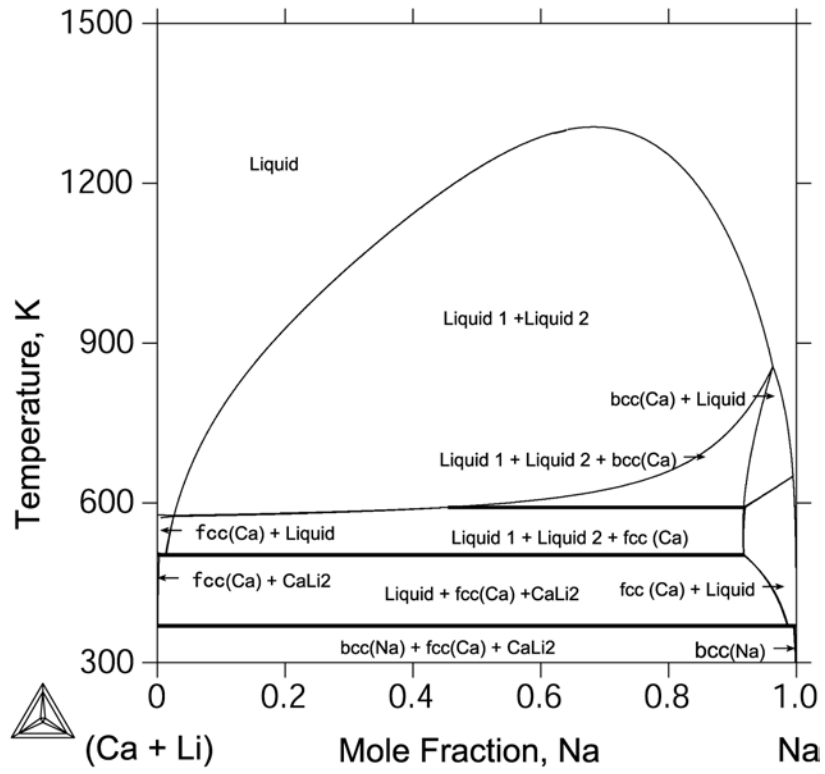
Fig. 6.21. Calculated isopleth section ($x_{Ca} = x_{Li}$).
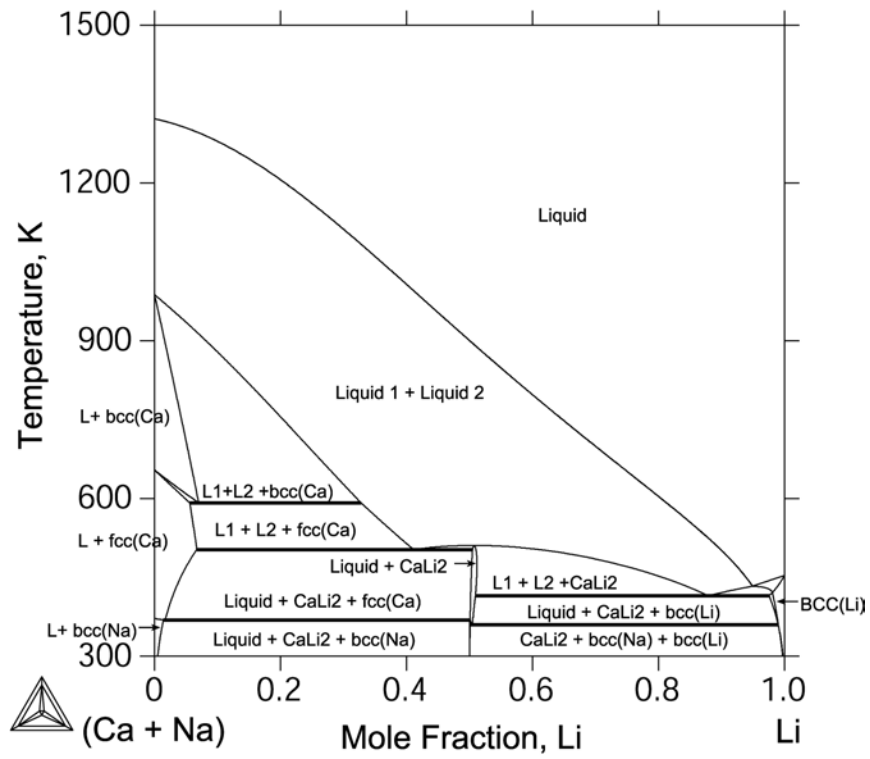
Fig. 6.22. Calculated isopleth section ($x_{Ca} = x_{Na}$).
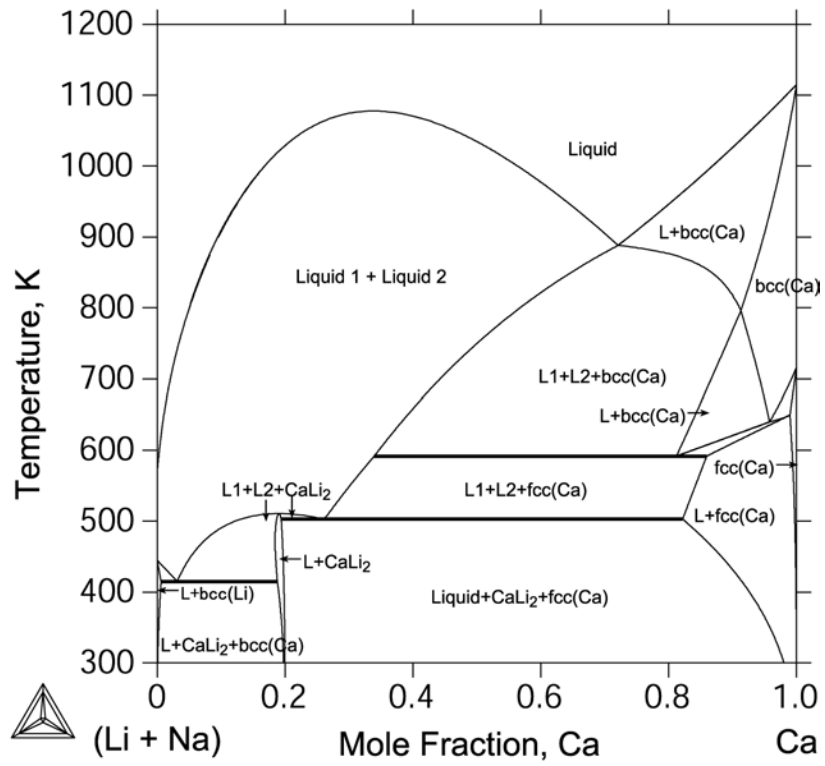
Fig. 6.23. Calculated isopleth section ($x_{Li} = x_{Na}$).

7. Thermodynamic Investigation of Sodium-Induced High-Temperature Embrittlement in Al-Mg Alloys

7.1 Introduction

Due to good formability, Al-Mg alloys are widely used in the automotive and aircraft industries. However, they suffer from poor hot rolling characteristics. Sodium is a common undesired impurity element in Al-Mg alloys of commercial grades. In spite of being present in trace amounts, sodium leads to HTE at 473 to 673 K as a result of intergranular fracturing and formation of cracks during the hot-rolling process [2, 3].

Ransley and Talbot [104] first investigated the embrittlement of Al-Mg-Si alloys by sodium and suggested that hot ductility is severely impaired with a sodium content higher than 20 ppm. In the reaction of $NaAlSi + 2Mg \rightarrow Al + Mg_2Si + Na_{free}$, a ternary compound, NaAlSi, was considered to be involved, resulting in free sodium in the form of atoms. The embrittlement is related to the adsorption of free sodium on internal surfaces generated in plastic flow and consequent modification of the growth of grain boundary cavities. Otsuka and Horiuchi [105] investigated the dependence of the hot ductility of Al-Mg alloys on temperature, strain rate, grain size and composition using the tensile test and found that the hot ductility trough shifts to higher temperatures with increasing strain rate and decreases with increasing grain size and bulk magnesium concentrations. However, the sodium content was not determined. Talbot and Granger [2] studied the effects of sodium and bismuth on HTE in Al-5Mg-0.15Si (wt %) and commercial Al-5Mg alloys by the use of a hydrogen absorption technique. They found that the solubility of sodium in Al-Mg alloys was about 5 ppm and that the excess sodium was in the form of free sodium atoms. However, Okada and Kanno's results [106], obtained in Al-5Mg and Al-5Mg-0.04Y alloys in the temperature range of 473 to 673 K, indicated that HTE was related to both hydrogen and sodium concentrations [100]. A concentration of 0.1 ppm of sodium was high enough to cause HTE.

Horikawa, Kuramoto, and Kanno [3, 11] examined the effect of sodium on HTE by measuring the reduction of area during tensile testing of specimens of a high-purity Al-5Mg alloy containing 0.01 to 1.8 ppm of sodium. The trace sodium content was detected by glow discharge mass spectrometry. They reported that the HTE disappeared completely when the sodium content was lower than 0.01 ppm. The trace sodium was assumed to segregate to the grain boundaries in the form of free sodium atoms and to reduce the grain boundary strength, although no sodium was detected on the intergranular fracture surface by auger electron spectroscopy (AES). However, Lynch [8] suggested that HTE is the result of the formation of low-melting-point sodium-rich phases or particles that precipitate at the grain boundaries of the alloys.

Despite numerous previous investigations, the mechanisms of sodium on HTE in Al-Mg alloys are still controversial [8, 9], partly because the trace amount of sodium cannot be detected, even by AES [11]. In the present work, efforts have been made to understand the mechanism and to reveal the correlations between HTE, phase formation, temperature, and composition by the use of thermodynamic modeling.

7.2   Phase Diagrams and Phase Evolution

To investigate the mechanism of sodium-induced HTE in Al-Mg alloys, it is very important to understand the correlations between HTE, phase relation, temperature, and constitution in Al-Mg alloys. These correlations can be explained through an understanding of the thermodynamics of the Al-Mg-Na system.

The thermodynamic database of the Al-Mg-Na system was developed by the present authors using the CALPHAD approach [107]. In the CALPHAD thermodynamic modeling, the Gibbs energies of individual phases are modeled through the coupling of phase diagrams and thermochemistry, and the model parameters are collected in thermodynamic databases. Models for the Gibbs energy of binary and ternary phases are primarily based on the crystal structure of the phases. The Gibbs energies of individual phases are expressed as a function of composition and temperature that can reveal the phase relations and phase compositions. In the present study, Thermo-Calc [100] was used for free-energy minimization, and the Al-Mg-Na database [107] was used for phase description.

Fig. 7.1 shows the calculated isopleth section of Al-5Mg alloys with respect to the sodium content. Note that the sodium content is plotted in the logarithmic scale because of its low values. There is a liquid miscibility gap in this system that originated from the Al-Na and Mg-Na systems, denoted by liquid-1 (aluminum-rich) and liquid-2 (sodium-rich). There is a two-phase region (liquid-2+fcc) between 524 and 853 K at fairly low sodium concentrations. The temperature and the sodium concentration range in this two-phase region coincide with the temperature and the sodium concentration zones in which HTE occurs, as will be shown later.

Further calculations were carried out to determine the relationship between the temperature and phase fractions for an Al-5Mg alloy containing 1.8 ppm of sodium. Fig. 7.2 shows phase evolution during cooling of the alloy. Upon cooling, the fcc phase begins to form at 908 K from the liquid-1 phase. Solidification is complete at 853 K, and the phase fraction of the fcc phase reaches 100%. When the fcc phase is cooled to 723 K, another liquid phase (liquid-2 phase) forms. The amount of the liquid-2 phase increases with decreasing temperature and can be as high as 2.1×10^{-6} mole fraction. This liquid-2 phase transforms to a bcc phase at 371 K. Fig. 7.3 shows the sodium content in the liquid-2 phase as a function of temperature, depicting that the liquid-2 phase is highly sodium-rich, and the sodium content increases with decreasing temperature.

Figs 7.2 and 7.3 indicate that sodium is completely dissolved in the aluminum-rich fcc phase in the temperature range of 723 to 853 K after solidification. As the temperature decreases, the highly sodium-rich liquid-2 phase forms from the solid fcc grains, most likely along grain boundaries or in other defect regions. Then, the liquid-2 phase transforms to the sodium-rich bcc phase at a low temperature.

7.3 Mechanism of Sodium-Induced HTE

The mechanism of sodium-induced HTE in Al-Mg alloys remains controversial. Talbot and Granger [2]; Ransley and Talbot [104]; and Horikawa, Kuramoto, and Kanno [3, 11] attributed HTE to primarily segregation of sodium atoms to grain boundaries, although no sodium was detected on intergranular fracture surfaces. Horikawa, Kuramoto, and Kanno [9] indicated that there is no possibility of forming enough sodium-rich particles or sodium-rich phases to cause HTE in view of the trace amount of sodium. Lynch [8] concluded that sodium-rich particles rather than sodium atoms at grain boundaries induce HTE in comparison to the case in Al-Li alloys [12, 13]. In this section, the mechanism of sodium-induced HTE is explained by describing the correlations between HTE, phase relation, temperature, and constitution in Al-Mg alloys.

Fig 7.4 shows the comparison between the calculated phase relations for the current study and the experimental data from the literature [3]. The calculated relationship between the temperature and the phase fraction for Al-5Mg-Na alloys under equilibrium conditions is shown in Fig. 7.4(a). The effect of trace sodium on the hot ductility of Al-5Mg alloys at different temperatures from the literature [3] is shown in Fig. 7.4(b), where the reduction of area is defined as the percentage decrease in the cross-sectional area of a tensile specimen caused by wasting or necking of the specimen. It is expressed as a percentage of the original area of the test piece and is a measure of ductility. In Fig. 7.4(a), it is evident that the sodium content significantly affects the formation temperature and the amount of liquid-2. With increasing sodium content in Al-5Mg-Na alloys, the amount of liquid-2 and its formation temperature increase. However, the temperature of transformation from the liquid-2 phase to the bcc phase does not change. The temperature is approximately equal to the melting temperature of pure sodium (371 K).

The ductility troughs in the temperature range of 400 to 700 K shown in Fig. 7.4(b) can be explained using the data from Fig. 7.4(a). The troughs start at about 700 K, at which point the liquid-2 phase starts to form. From 700 to 600 K, as the amount of liquid-2 increases, the reduction of area decreases. At about 550 K, the amount of liquid-2 reaches the maximum, and the reduction of area reaches the minimum. At temperatures lower than 524 K, the β (Al$_3$Mg$_2$) phase forms and partially blocks the liquid-2's access to grain boundaries. At about 380 K, the liquid-2 phase completely transforms to bcc, and hot ductility recovers almost completely.

To illustrate the mechanism of HTE caused by sodium, hot ductility and the amount of the liquid-2 phase in Al-5Mg alloys at 573 K are plotted as a function of the sodium content in Fig. 7.5. One can see that with more liquid-2 phase, the HTE becomes more severe. When the sodium content is 0.01 ppm, the mole fraction of the liquid-2 phase is almost equal to zero and hardly affects the ductility of the alloy at elevated temperatures. This result is consistent with the experimental investigations performed by Horikawa, Kuramoto, and Kanno [3, 11].

7.4 Suppression of Sodium-Induced HTE in Al-Mg Alloys

It is generally understood that sodium content has to be extremely low to completely suppress HTE and avoid cracking. On the other hand, contamination with sodium is inevitable in the normal manufacturing process of Al-Mg alloys. Because HTE is closely related to the liquid-2 phase formation, HTE can be suppressed by avoiding the liquid-2 phase formation in the alloy.

We define the hot-rolling safe zone as the region on the phase diagram in which only the fcc phase exists and the HTE sensitive zone as the one in which the liquid-2 phase exists.

Fig 7.6 is an enlarged view of Fig. 7.5. It shows the HTE sensitive and safe zones in a temperature vs. sodium-content diagram of Al-5Mg-Na alloys. The hot-rolling safe zone is bounded by the maximum hot-rolling temperature line and the dashed line shown in Fig. 7.6. The HTE sensitive zone is bounded by the maximum temperature line at which the liquid-1 phase transforms to fcc, the bcc/liquid-2 transformation temperature line, and the dashed line. The dashed line on Fig. 7.6 is also the boundary between the hot-rolling safe zone and the HTE sensitive zone. In the hot-rolling safe zone at the left side of the dashed line, no liquid-2 phase forms, and the single-phase fcc microstructure guarantees good hot-rolling characteristics. HTE can be avoided when Al-5Mg-Na alloys are hot rolled in this zone. However, in the HTE sensitive zone at the right side of the dashed line, the liquid-2 phase is most likely to occur at the grain boundaries and reduces hot-rolling formability. For Al-5Mg-Na alloys containing different sodium contents, the hot-rolling temperature should be chosen from above the dashed line to suppress HTE and avoid cracking. For a given sodium content, there is a critical temperature above which high-temperature cracking tends to occur during hot rolling. For instance, the critical temperature of the Al-5Mg alloy containing 1 ppm sodium is 689 K. That is to say that the hot-rolling temperature should be higher than 689 K to avoid HTE. If the sodium content decreases to 0.1 ppm, the critical temperature decreases to 583 K. Therefore, the lower the sodium content, the lower the critical temperature. As a result, hot rolling can be performed at lower temperatures for alloys containing less sodium than those containing more sodium. The maximum hot-rolling temperature is 853 K, above which the aluminum-rich liquid-1 phase and fcc phase coexist (i.e., the Al-5Mg alloy begins to melt).

The boundaries that define the HTE zone shown in Fig. 7.6 include the critical hot-rolling temperature (dashed line), the maximum hot-rolling temperature, and the maximum sodium content. These boundaries can be affected by varying the magnesium content of the alloy.

The critical hot-rolling temperature is illustrated as the dashed line separating the hot-rolling safe zone and the HTE sensitive zone in Fig. 7.6. Fig. 7.7 shows the relationship between the critical hot-rolling temperature and the magnesium content of the alloy. With increasing magnesium content, the hot-rolling safe zone becomes smaller in terms of the Na content. An expression for the critical hot-rolling temperature, T, in the range of magnesium content of $0.01 \leq w_{Mg} \leq 0.10$ is given in Eq. (25) by the use of regression analysis:

$$\frac{10^4}{T(K)} = -1.27 - 1.91 w_{Mg} - (1.09 + 1.19 w_{Mg}) \ln(w_{Na}), \tag{25}$$

where w_{Na} and w_{Mg} are the weight fractions of sodium and magnesium. The logarithmic relationship shown in Eq. (25) for the sodium content indicates the critical role of sodium in HTE.

The maximum hot-rolling temperature, T^{Max}, for magnesium content in the range of $0.01 \leq w_{Mg} \leq 0.10$ can be expressed as shown in Eq. (26) below.

$$T^{Max}(K) = 931 - 1527w_{Mg} \qquad (26)$$

The maximum hot-rolling temperature is also the upper limit of the HTE zone shown in Fig. 7.6. The line defined by Eq. (26) is illustrated in Fig.7.7. The liquid-1 phase forms in the alloy when the temperature is higher than the maximum hot-rolling temperature.

The maximum sodium content shown in Fig. 7.6 is a critical composition point above which the liquid-2 phase always forms at any hot-rolling temperatures. Therefore, HTE cannot be avoided when the sodium content is higher than the maximum sodium content. The relationship between the maximum sodium content, w_{Na}^{Max}, and the magnesium content is shown in Fig. 7.7 and can be expressed by Eq. (27) below.

$$w_{Na}^{Max}(\text{ppm}) = 16.47 - 94.84w_{Mg} \qquad (27)$$

Also, the maximum sodium content decreases with increasing magnesium content.

The curves in Fig. 7.7 are the calculated results using Eqs. (25) to (27), respectively. The symbols are the data points calculated using the Thermo-Calc software and Al-Mg-Na database. It is clear that the results obtained using Eqs. (25) and (27) agree well with the thermodynamic simulation results . Thus, Eqs. (25), (26), and (27) can be used to determine the critical hot-rolling temperature, the maximum hot-rolling temperature, and the maximum sodium content. The hot-rolling safe zone of the Al-Mg-Na alloys can be defined using these boundary equations.

Fig 7.8 is a contour map of the critical hot-rolling temperature and the maximum sodium content (dashed line) of Al-Mg-Na alloys with respect to magnesium and sodium contents. The contour map can serve as a roadmap for Al-Mg alloys processing by enabling one to choose the proper hot-rolling temperature according to various magnesium and sodium contents. To avoid cracking formation during the hot-rolling operation, the rolling temperature has to be higher than the critical hot-rolling temperature illustrated in Fig. 7.8.

7.5   Cracking Tendency of Al-Mg Alloys in the HTE Sensitive Zone

The hot-rolling safe zone was discussed in detail in Sect. 7.4. Ideally, the alloy should be hot rolled in this zone to avoid cracking formation. In case the alloy has to be hot rolled at the temperature range corresponding to that of the HTE sensitive zone, the cracking tendency, or the extent of HTE, of the alloy can be altered by changing the hot-rolling temperature. The tendency of cracking formation can be evaluated by the use of the mole fraction of the liquid-2 phase because the reduction of area, a measure of ductility, decreases with increasing mole fraction of the liquid-2 phase, as shown in Fig. 7.4.

Figure 7.9 shows the relationship between the mole fraction of the liquid-2 phase and the processing temperature for Al-5Mg-Na alloys. There are two vertical lines on Fig. 7.9—one representing the maximum hot-rolling temperature and the other the liquid-2/bcc transformation temperature. Usually alloys are hot rolled at temperatures between these two temperatures. When the temperature is higher than the maximum hot-rolling temperature, liquid-1 phase forms (see

Fig. 7.1). Generally the mole fraction of the liquid-2 increases substantially with increasing sodium content. As a result, the cracking tendency of the alloys also increases substantially with increasing sodium content. However, the mole fraction of the liquid-2 phase decreases slightly with increasing temperature in the temperature range between 371 K and about 650 K. At temperatures higher than 650 K, the mole fraction decreases sharply with temperature. These facts suggest that the cracking tendency is not sensitive to the processing temperature in the temperature range of 371 to 650 K, but decreases with increasing processing temperature in the temperature range of 650 to 853 K. For alloys containing less sodium, for instance 1 ppm, the mole fraction of the liquid-2 phase decreases with increasing processing temperature, reaches zero at 689 K, and remains at zero at temperatures between 689 and 853 K, which is the temperature range of the hot-rolling safe zone of this alloy. For the alloy containing 5 wt % magnesium and 11.35 ppm sodium, the mole fraction of the liquid-2 phase reaches zero only at 853 K, indicating an extremely small temperature range of the HTE zone when the sodium content is close to 11.35 ppm. In cases in which an Al-5Mg-Na alloy contains more than 11.35 ppm sodium, liquid phases exist when the processing temperature is higher than 371 K, the liquid-2/bcc transformation temperature. These alloys have to be processed at high temperatures (but lower than 853 K) to reduce the cracking tendency during hot-rolling operations.

For a given mole fraction of the liquid-2 phase, the cracking tendency of the alloy is dependent on the size of the fcc grains because the size of the liquid-2 phase film is dependent on the fcc grain size. The liquid-2 phase usually occurs at the grain boundaries. Because the mole fraction of the liquid-2 phase is so small, it is difficult to form a continuous liquid film at the grain boundaries. For the ease of analysis, the authors assume that the liquid-2 phase occurs at the grain boundaries as a continuous film. Thus, the thickness of the liquid film is a measure of cracking tendency because it is proportional to the size of the discontinuous liquid phase at the grain boundaries.

Assuming that the mole fraction of the liquid-2 phase is equal to its volume fraction and that the grain boundaries are covered by a continuous layer of the liquid phase, the volume fraction of the liquid-2 phase is given by the following equation:

$$f_{liquid-2} = \frac{V_{liquid-2}}{V_g + V_{liquid-2}} = \frac{\delta S_g}{V_g + \delta S_g}, \tag{28}$$

where $V_{liquid-2}$ is the volume of the liquid-2 phase, V_g the volume of the fcc grains, S_g the surface area of the grains, and δ the average thickness of the liquid-2 film. In three dimensions, according to Tomkeieff's theorem [108], the volume of the grains can be expressed as follows:

$$V_g = \frac{S_g L}{4}, \tag{29}$$

where L is the average intercept length of grains, which is proportional to the grain size.

Using Eq. (29) in Eq. (28), we obtain Eq. (30) below.

$$f_{liquid-2} = \frac{\delta S_g}{V_g + \delta S_g} = \frac{\delta S_g}{S_g L / 4 + \delta S_g} = \frac{4\delta}{L + 4\delta} \approx \frac{4\delta}{L} \tag{30}$$

Thus, the thickness of the liquid-2 phase film can be calculated by the following equation,

$$\delta = 0.25 \cdot L \cdot f_{liquid-2}, \tag{31}$$

where $f_{liquid-2}$ is the mole fraction of the liquid-2 phase and is approximately equal to the sodium content, as shown in Fig. 7.4(a). From Eq. (31), one can see that with increasing grain size, the thickness of the liquid-2 phase film increases and HTE becomes more pronounced. As a result, alloys with small grains tend to have improved HTE resistance.

The thickness of the liquid-2 phase calculated by the use of Eq. (31) seems to be extremely thin. For example, with a typical grain size of $300\,\mu m$ [3, 11], the average thickness of the liquid film is about 0.75 Å according to Eq. (31) when $f_{liquid-2} = 1\,ppm$. At such a small liquid fraction, the liquid film is not likely to be continuous. Instead, small pockets of thin liquid film may occur at grain boundaries, however, they would be difficult to be detected by the use of AES.

7.6   Summary

A fundamental understanding of sodium-induced HTE in Al-Mg-Na alloys can be gained by performing thermodynamic investigations. The results indicate that the liquid miscibility gap due to sodium has an important effect on HTE. A liquid-2 phase forms from the solid fcc phase (most likely at grain boundaries) during cooling, resulting in the occurrence of HTE. A comparison of the thermodynamic simulation results from experimental measurements on the high-temperature ductility of Al-5Mg-Na alloy shows that HTE occurs in the temperature range in which the liquid-2 phase exists.

A hot-rolling safe zone is defined in which no liquid-2 phase will occur, and an HTE sensitive zone is defined on the phase diagram where the liquid-2 phase forms. The hot-rolling safe zone is within the temperature and composition ranges described using Eqs. (33) and (34):

$$\frac{10^4}{T(K)} = -1.27 - 1.91w_{Mg} - (1.09 + 1.19w_{Mg})\ln(w_{Na}), \tag{33}$$

$$T^{Max}(K) = 931 - 1527w_{Mg}, \tag{34}$$

where $T(K)$ is the critical hot-rolling temperature, and T^{Max} is the maximum hot-rolling temperature. The hot-rolling safe zone lies on the left of the $T(K)$, and w_{Mg} and w_{Na} and the HTE sensitive zone lie on the right side. HTE should not occur when the hot-rolling temperature and the composition of the alloy fall in the safe zone. In the HTE sensitive zone, the tendency of crack formation is proportional to the mole fraction of the liquid-2 phase and the size of the fcc grains. The cracking tendency decreases with decreasing sodium content, increasing hot-rolling temperature (in the temperature range between 371 and T^{Max}), and decreasing grain size.
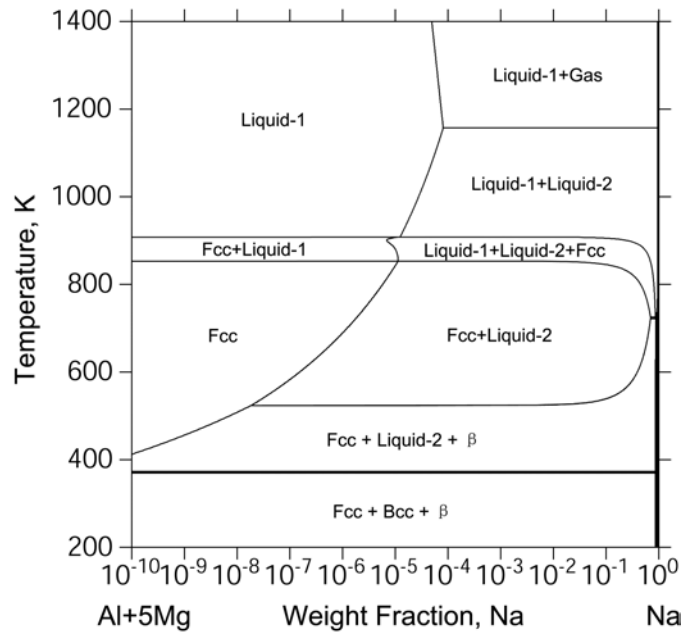
Fig. 7.1. Calculated isopleth section (Al-5Mg-Na).
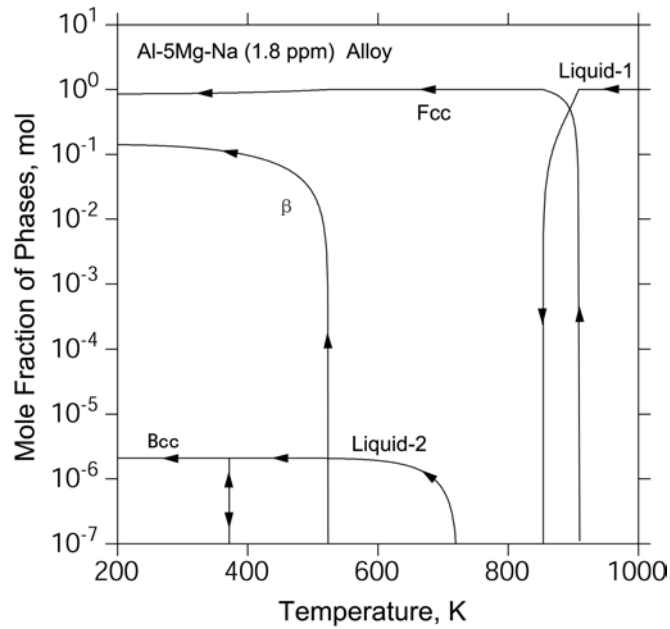
Fig. 7.2. Calculated mole fraction of each phase vs. temperature curves during the solidification of the Al-5Mg-Na (1.8 ppm) alloy.

48
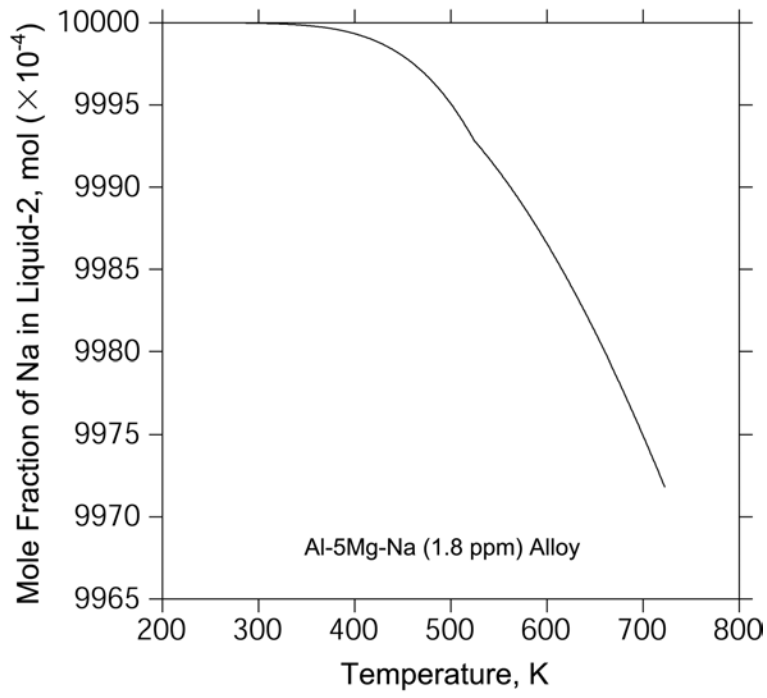
Fig. 7.3. Sodium content in the liquid-2-phase-vs.-temperature curve for the Al-5Mg-Na (1.8 ppm) alloy.
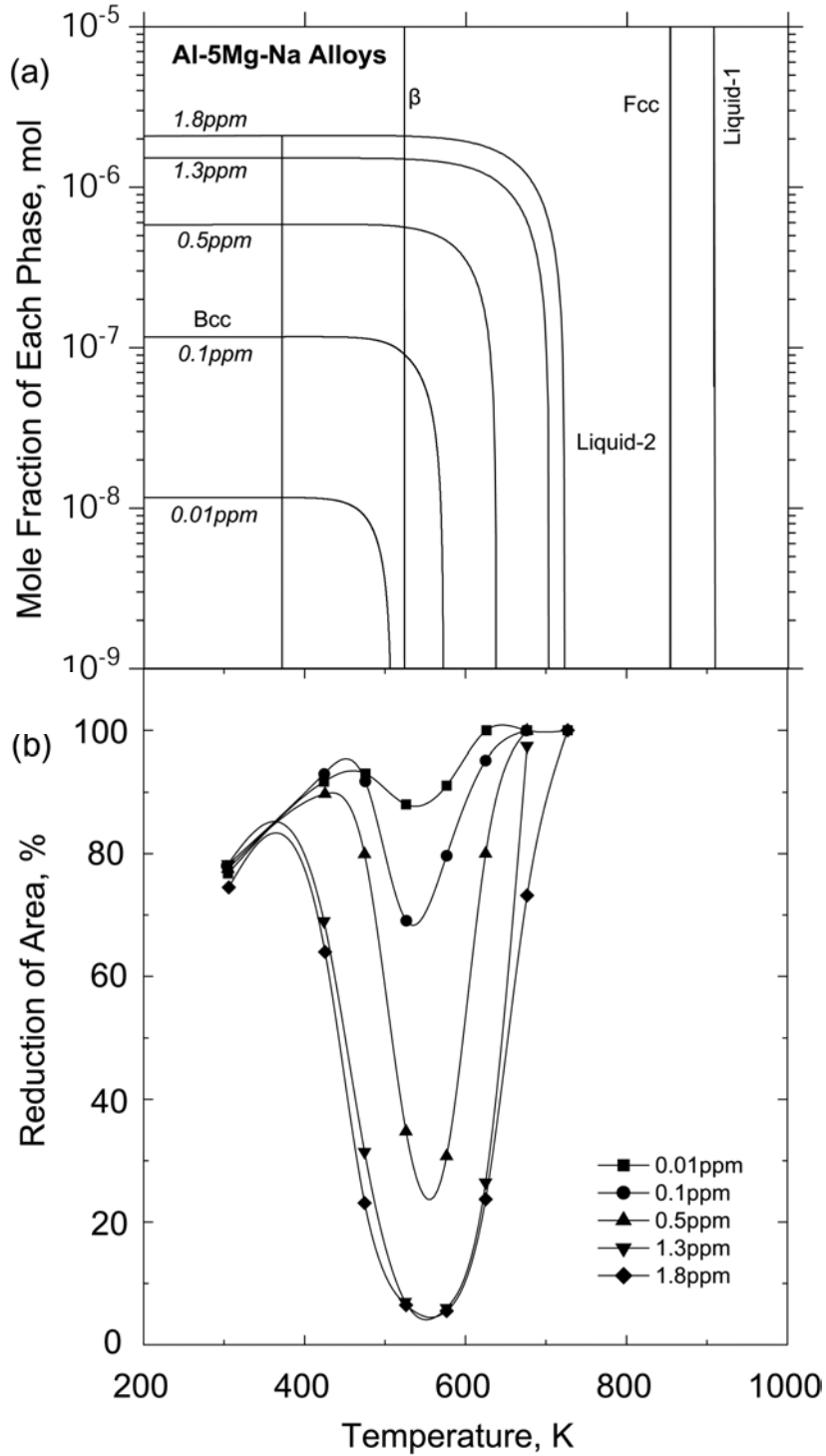
Fig. 7.4. Calculated phase relations in comparison with the experimental data on the reduction of area [3]. (a) Calculated mole fraction of each phase-vs.-temperature curve during the solidification of Al-5Mg-Na alloys with different sodium contents; (b) effect of sodium on hot ductility of Al-5Mg alloys at different temperatures [3].
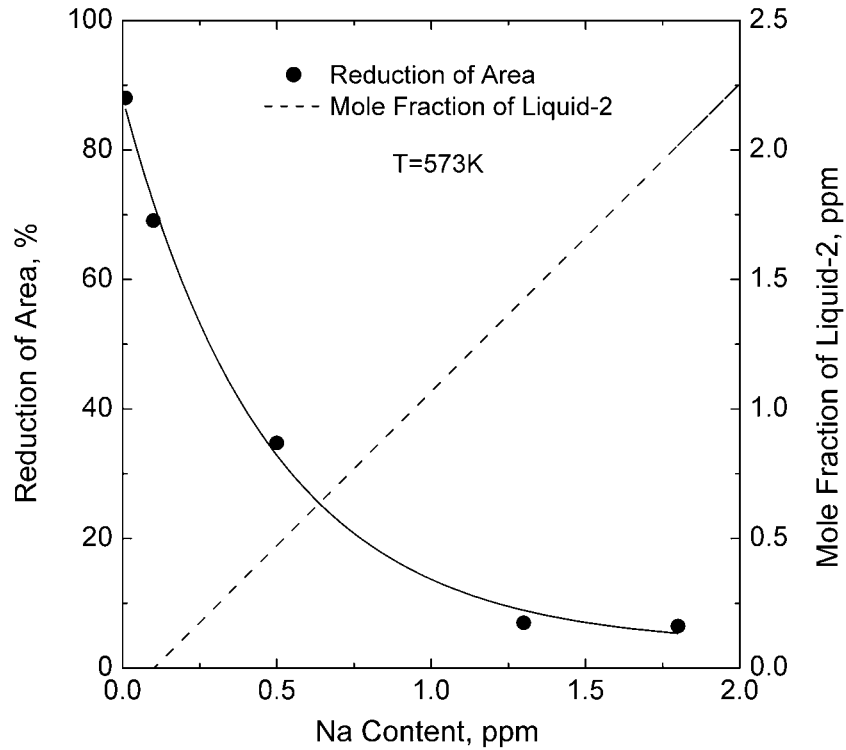
Fig. 7.5. Experimental hot ductility ● [3] and the calculated amount of the liquid-2 phase of Al-5Mg-Na alloys plotted as a function of the sodium content.
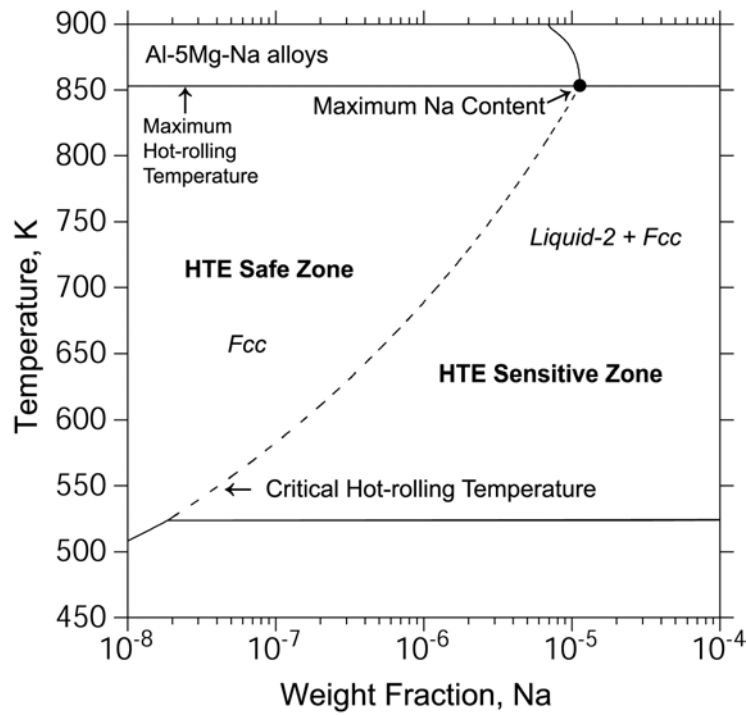
Fig. 7.6. HTE sensitive and safe zones as well as critical hot-rolling temperatures (the dashed line) and maximum sodium content of Al-5Mg-Na alloys.
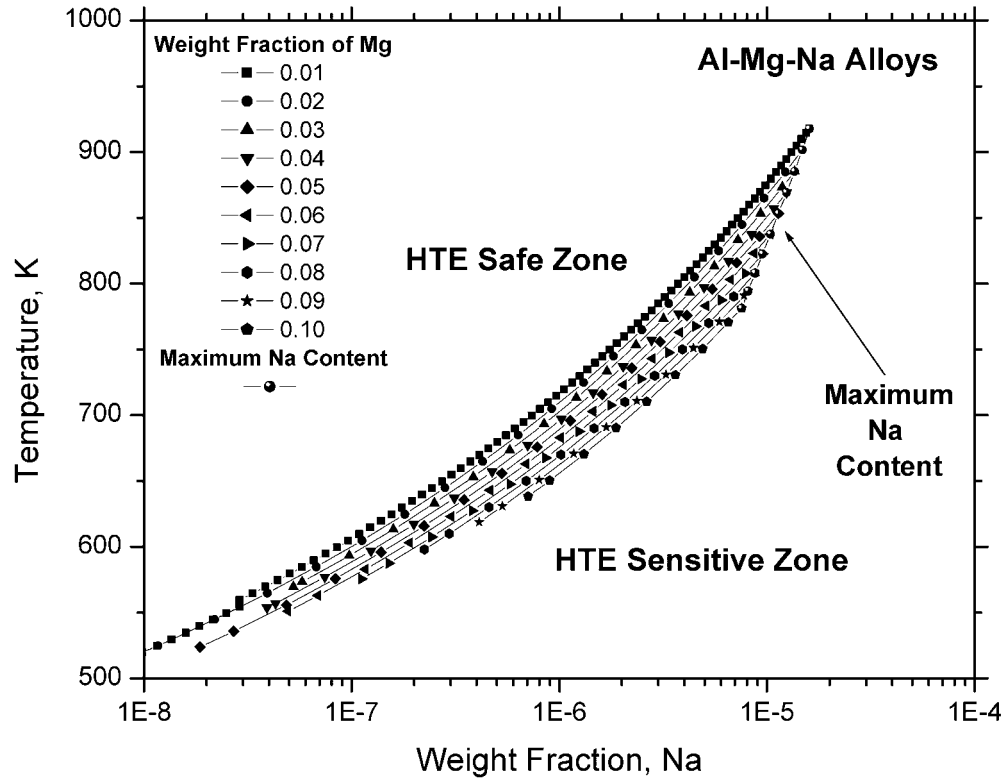
Fig. 7.7. HTE sensitive and safe zones as well as critical hot-rolling temperatures and maximum sodium content of the Al-Mg-Na alloys with different magnesium contents.
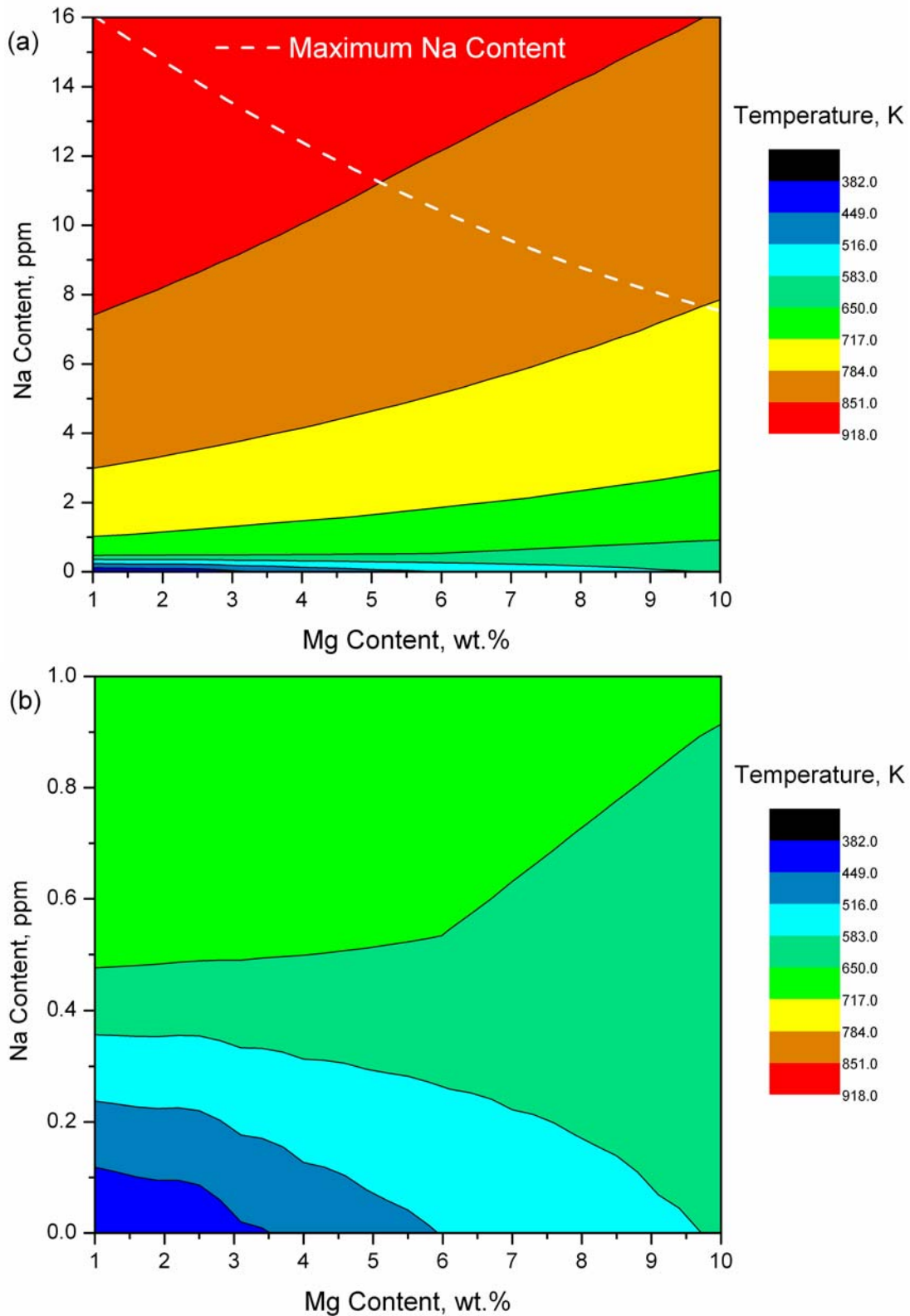
Fig. 7.8. Contour map of the critical hot-rolling temperature and the highest sodium content (the dashed line) of Al-Mg alloys with respect to magnesium and sodium content (a) and with the y-axis enlarged (b).
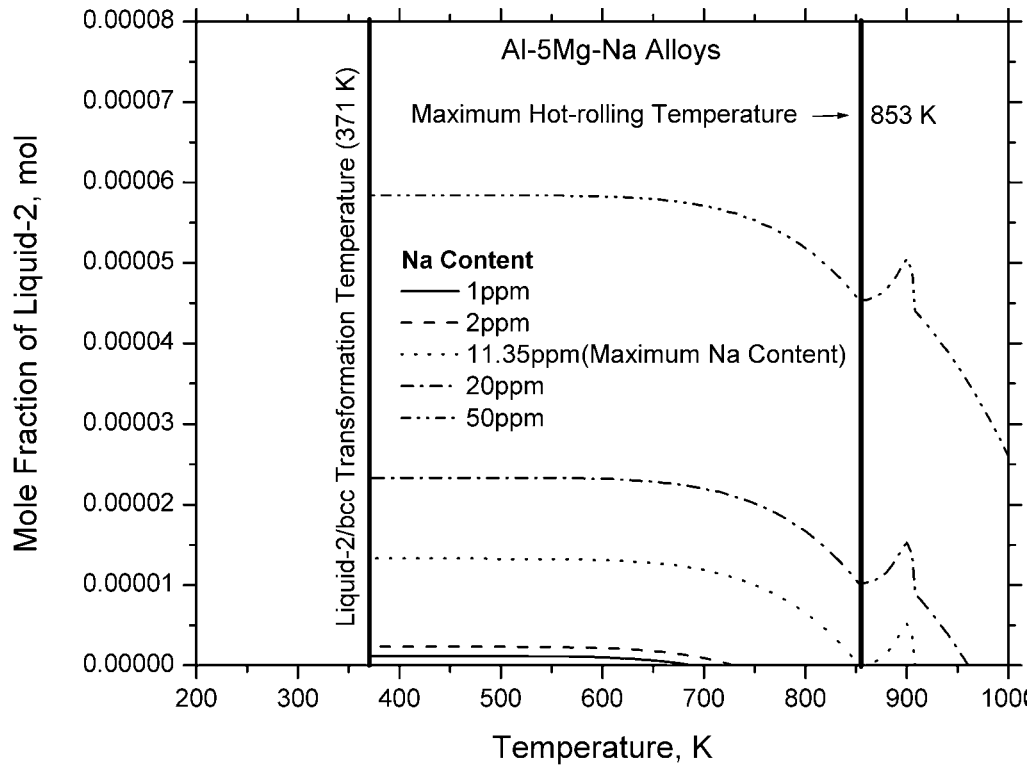
Fig. 7.9. Relationship between the calculated mole fraction of the liquid-2 phase and the processing temperature at various sodium contents of the Al-5Mg-Na alloy (1.8 ppm).

8. Accomplishments

8.1 Patents

N/A

8.2 Publications and Presentations

8.2.1 Publications

1. Shengjun Zhang, Qingyou Han and Zi-Kui Liu. *Fundamental understanding of Na-induced high temperature embrittlement in Al-Mg alloys*, Philo. Mag., Vol.87, 2007, 147-157.

2. Shengjun Zhang, Carl Brubaker, Chao Jiang, Mei Yang, Yu Zhong, Qingyou Han and Zi-Kui Liu. *A combined first-principles calculations and thermodynamic modeling of the F-K-Na system*, Mater. Sci. Eng. A, Vol.418, 2006, 161-171.

3. Shengjun Zhang, Qingyou Han and Zi-Kui Liu. *Thermodynamic modeling of the Al-Mg-Na system*, J. Alloy. Compd., Vol.419, 2006, 91-97.

4. Shengjun Zhang, Dongwon Shin and Zi-Kui Liu. *Thermodynamic modeling of the Ca-Li-Na system*, Calphad, Vol.27, 2003, 235-241.

8.2.2 Presentations

The presentations listed here are all given by S. Zhang. The results from this project are also presented many times by Dr. Zi-Kui Liu in many invited presentations and teaching of Thermodynamics of Materials to illustrate the principles and applications of computational thermodynamics.

1. S. Zhang, Q. Han, and Z.-. Liu ,"Thermodynamic Investigation of the Effect of Na on High-Temperature Embrittlement of Al-Mg Alloys," 2006 TMS Annual Meeting & Exhibition, San Antonio, Texas, USA, March 12–16, 2006.

2. S. Zhang, Q. Han, and Z.-. Liu ,"Effects of Impurities in Aluminum Alloys Processing," 2004 TMS Annual Meeting & Exhibition, Charlotte, North Carolina, USA, March 14–18, 2004.

3. S. Zhang, and Z.-K. Liu "Thermodynamic Modeling of the Al-Mg-Na System," 2004 TMS Annual Meeting & Exhibition, Charlotte, North Carolina, USA, March 14–18, 2004.

4. S. Zhang, D. Shin, and Z.-K. Liu ,"Thermodynamic Modeling of the Ca-Li-Na System," International Conference on Phase Diagram Calculations and Computational Thermodynamics (Calphad XXXII), La Malbaie, Québec, Canada, May 25–30, 2003.

8.3 Technology Transfer

Intellectual property has been generated from this significant effort. A thermodynamic database has been developed. The thermodynamic database covers aluminum alloys containing sodium, calcium, magnesium, lithium, and potassium. Most of these elements are not included in commercial thermodynamic database. The research team is interacting with ThermoCalc, Inc. on licensing issues.

8.4 Education

The PhD study of Shengjun Zhang was supported by this project. Dr. Zhang's PhD degree was awarded in August 2006. He is currently a postdoctoral fellow in Northwestern University.

9. Summary and Conclusions

Aluminum alloys are widely used in the automobile and aerospace industries as structural materials because of their light weight, high strength, and good formability. However, they suffer from the poor hot-rolling characteristics as a result of undesired impurities such as calcium, lithium, potassium, and sodium. Although these elements have been identified as detrimental impurities for the extruded aluminum alloys, no systematic theoretical research has been carried out to investigate the behavior of these impurities during aluminum alloy processing. Moreover, these four elements are not included in the existing commercial aluminum alloys databases.

In this study, the thermodynamics of the Al-Ca-Li-Mg-Na-K system were modeled using a combined CALPHAD and first-principles approach. Each phase was described using the proper thermodynamic model according to its crystal structure and physical properties. The enthalpies of formation of phases were provided by first-principles method as complements to the experimental data. SQSs were applied to model the substitutionally random alloys. Self-consistent thermodynamic parameters were obtained.

Based on the developed database, a thermodynamic investigation was carried out to reveal the correlations between HTE, phase relations, temperature, and sodium content of Al-Mg alloys in this work. The HTE sensitivity and safe zones of the Al-Mg alloy in terms of temperature and sodium content were determined. The effect of sodium on hot ductility loss was also studied. A new method was presented that controls hot-rolling temperature to suppress HTE and avoid cracking.

Energy and environmental benefits from the results of this project can accrue from reduced rejection rates of the aluminum sheet and bar. The sheet and extruded bar quantities produced in the United States during 2000 were 10,822 million and 4,546 million pounds. It is assumed that 50% of the sheet and 10% of the bar will be affected by the project's results. With the current process, the rejection rate of sheet and bar is estimated to be 5%. Assuming that at least half of the 5% rejection of sheet and bar will be eliminated by using the results of this research and that 4% of the aluminum will be lost through dross (Al_2O_3) during remelting of the reject, full-scale industrial implementation of the project results would lead to energy savings in excess of 6.2 trillion Btu per year and cost savings of $42.7 million by 2020.

10. Recommendations

10.1 Database Development Associated with Potassium

Potassium is a very important impurity element in aluminum alloys. Although the potassium content is lower than the sodium content, potassium is one of the alkali metals that cause embrittlement in Al-Li alloys; however, the mechanism is still uncertain. The thermodynamic database will be the basis for further investigations. The Al-K, Mg-K, Li-K, and Ca-K binary systems can be modeled using CALPHAD combined with first-principles methods, as demonstrated in the present work. The binary system associated with potassium are fairly simple without intermetallic compounds and with liquid miscibility gaps. The solubility of potassium in aluminum, magnesium, lithium, and potassium are very tiny. Because the experimental information about these binary systems is very sparse, first-principles calculations become increasingly important and can provide more information.

10.2 Thermodynamic Investigation of HTE of Al-Mg Alloys Caused by Calcium and Lithium

Although the effect is much milder than that of sodium, small amounts of calcium and lithium can bring about HTE in Al-Mg alloys. The mechanism is still uncertain. The databases of the Al-Mg-Ca and Al-Mg-Li systems have been developed. Thermodynamic equilibrium calculations show that no liquid is present in the temperature range of the HTE. Further investigations will be carried out to analyze the mechanisms in the presence of sodium.

10.3 Thermodynamic Investigation of HTE of Al-Li Alloys Caused by Sodium and Potassium

Being low-melting-point impurities, sodium and potassium in Al-Li alloys are shown to occur as discrete lenticular particles along the grain boundaries. They were found to have little effect on the toughness or ductility of high-purity aluminum. The detrimental effects exist only in alloys containing amounts of lithium and magnesium. Thermodynamic investigations will be carried out to reveal the correlations between HTE, phase relations, temperature, and contents of impurities in the Al-Mg alloys with small amount of sodium and potassium.

10.4 Integration of Binary Impurity Data with the Commercial Aluminum Databases

The commercial aluminum-based database (TTAl3, version 3.0, February 2000) was developed by Thermotech Ltd. and presents a comprehensive database for aluminum alloys with a proven track record. This database contains 15 elements (Al, B, C, Cr, Cu, Fe, Mg, Mn, Ni, Si, Sr, Ti, V, Zn, and Zr) and more than 40 phases in aluminum alloys. It can be used for all major types of commercial aluminum alloys, ranging from commercial pure aluminum to complex alloys such as AA339.1, AA7075. This database has been widely and successfully used. However, the important impurity elements such as calcium, lithium, sodium, and potassium are not included in this database, and it cannot be used to solve the industry problems associated with these alkali

and alkaline earth metals. The Al-Ca-Li-K-Mg-Na database created in the present work can be integrated with TTAl3 to generate a database with 19 elements for understanding and improving processing of commercial Al alloys.

11. References

1. R. Narayanan and Y. Sahai, "Metal Loss in Aluminium Alloys in Molten Salt Fluxes," *Light Met.*, Las Vegas, NV,USA, **TMS, Warrendale, PA, USA**, 1995, pp. 803-807.
2. D. E. J. Talbot and D. A. Granger, "Research Summary: Effects of Sodium and Bismuth in Aluminum-Magnesium Alloys," *JOM,* Vol.47, 1995, 44-46.
3. K. Horikawa, S. Kuramoto and M. Kanno, "Sources of a Trace Amount of Sodium and its Effect on Hot Ductility of an Al-5 mass% Mg alloy," *Light Met. Rev.,* Vol.7, 2000, 18-23.
4. J. E. Hatch, *Aluminum: Properties and Physical Metallurgy,* American Society For Metals, Metals Park, Ohio, 1984.
5. X. Li, X. Rao, D. Zhang and P. Si, "Corrosion Behavior of Aluminum-Magnesium Alloys in Molten Sodium," *Transaction of Nonferrous Metals Society of China (English Edition),* Vol.10, 2000, 224-227.
6. G. D. Parkes, *Mellor's Modern Inorganic Chemistry,* John Wiley and Sons, Inc., New York, 1967.
7. C. Rosenkilde, L. H. Arnesen and O. Wallevik, "Determination of the Henrian activity coefficient of sodium in liquid magnesium," *J. Phase Equilib.,* Vol.21, 2000, 521-527.
8. S. P. Lynch, "Comments on "Intergranular fracture caused by trace impurities in an Al-5.5 mol% Mg alloy"," *Scr. Mater.,* Vol.47, 2002, 125-129.
9. K. Horikawa, S. Kuramoto and M. Kanno, "Reply to comments on "Intergranular fracture caused by trace impurities in an Al-5.5 mol% Mg alloy"," *Scr. Mater.,* Vol.47, 2002, 131-135.
10. K. Horikawa, H. Okada and M. Kanno, "Effect of small amount of lithium on hot ductility of Al-Mg base alloys," *Aluminium Alloys: Their Physical and Mechanical Properties, Pts 1-3*, Zurich-Uetikon, **Transtec Publications Ltd**, 1996, pp. 1181-1186.
11. K. Horikawa, S. Kuramoto and M. Kanno, "Intergranular fracture caused by trace impurities in an Al-5.5 mol% Mg alloy," *Acta Mater.,* Vol.49, 2001, 3981-3989.
12. D. Webster, "The Effect of Low Melting-Point Impurities on the Properties of Aluminum-Lithium Alloys," *Metall. Trans. A,* Vol.18A, 1987, 2181-2193.
13. E. D. Sweet, S. P. Lynch, C. G. Bennett, R. B. Nethercott and I. Musulin, "Effects of alkali-metal impurities on fracture toughness of 2090 Al-Li-Cu extrusions," *Metall. Trans. A,* Vol.27A, 1996, 3530-3541.
14. L. Kaufman and H. Bernstein, *Computer Calculation of Phase Diagram with Special Reference to Refractory Metals,* Academic Press, New York, 1970.
15. L. Kaufman, "Computational thermodynamics and materials design," *CALPHAD,* Vol.25, 2001, 141-161.
16. A. T. Dinsdale, "SGTE Data for Pure Elements," *CALPHAD,* Vol.15, 1991, 317-425.
17. O. Redlich and A. T. Kister, "Algebraic Representations of Thermodynamic Properties and the Classification of Solutions," *Ind. Eng. Chem.,* Vol.40, 1948, 345-348.
18. M. Hillert, B. Jansson, B. Sundman and J. Agren, "A Two-Sublattice Model for Molten Solutions with Different Tendency for Ionization," *Metall. Trans. A,* Vol.16A, 1985, 261-266.

19. B. Sundman, "Modification of the Two-Sublattice Model for Liquid," *CALPHAD,* Vol.15, 1991, 109-119.

20. W. Kohn and L. J. Sham, "Self-Consistent Equations Including Exchange and Correlation Effects," *Phys. Rev. A,* Vol.140, 1965, 1133.

21. D. M. Ceperley and B. J. Alder, "Ground State of the Electron Gas by a Stochastic Method," *Phys. Rev. Lett.,* Vol.45, 1980, 566.

22. A. Zunger, S. H. Wei, L. G. Ferreira and J. E. Bernard, "Special quasirandom structures," *Phys. Rev. Lett.,* Vol.65, 1990, 353-356.

23. S. H. Wei, L. G. Ferreira, J. E. Bernard and A. Zunger, "Electronic properties of random alloys: Special quasirandom structures," *Phys. Rev. B,* Vol.42, 1990, 9622-9649.

24. K. C. Hass, L. C. Davis and A. Zunger, "Electronic Structure of Random Al0.5Ga0.5As alloys: Test of the "special-quasirandom-structures" description," *Phys. Rev. B,* Vol.42, 1990, 3757-3760.

25. Z. W. Lu, S. H. Wei and A. Zunger, "Large lattice-relaxation-induced electronic level shifts in random Cu1-xPdx alloys," *Phys. Rev. B,* Vol.44, 1991, 3387-3390.

26. Z. W. Lu, S. H. Wei and A. Zunger, "Electronic Structure of Ordered and Disordered Cu3Au and Cu3Pd," *Phys. Rev. B,* Vol.45, 1992, 10314-10330.

27. A. V. Ruban, S. I. Simak, S. Shallcross and H. L. Skriver, "Local lattice relaxations in random metallic alloys: Effective tetrahedron model and supercell approach," *Phys. Rev. B,* Vol.67, 2003, 214302.

28. V. Ozolins, C. Wolverton and A. Zunger, "Cu-Au, Ag-Au, Cu-Ag, and Ni-Au intermetallics: First-principles study of temperature-composition phase diagrams and structures," *Phys. Rev. B,* Vol.57, 1998, 6427-6443.

29. C. Wolverton, "Crystal structure and stability of complex precipitate phases in Al-Cu-Mg-(Si) and Al-Zn-Mg alloys," *Acta Mater.,* Vol.49, 2001, 3129-3142.

30. C. Jiang, C. Wolverton, J. Sofo, L. Q. Chen and Z. K. Liu, "First-principles study of binary bcc alloys using special quasirandom structures," *Phys. Rev. B,* Vol.69, 2004, 214202.

31. P. E. Blochl, "Projector augmented-wave method," *Phys. Rev. B,* Vol.50, 1994, 17953-17979.

32. G. Kresse and J. Joubert, "From ultrasoft pseudopotentials to the projector augmented wave method," *Phys. Rev. B,* Vol.59, 1999, 1758.

33. G. Kresse and J. Furthmuller, "Efficient iterative schemes for ab initio total-energy calculations using a plane-wave basis set," *Phys. Rev. B,* Vol.54, 1996, 11169-11186.

34. G. Kresse and J. Furthmuller, "Efficiency of ab-initio total energy calculations for metals and semiconductors using a plane-wave basis set," *Comput. Mater. Sci.,* Vol.6, 1996, 15-50.

35. J. P. Perdew, J. A. Chevary, S. H. Vosko, K. A. Jackson, M. R. Pederson, D. J. Singh and C. Fiolhais, "Atoms, molecules, solids, and surfaces: Applications of the generalized gradient approximations for exchange and correlation," *Phys. Rev. B,* Vol.46, 1992, 6671-6687.

36. H. J. Monkhorst and J. D. Pack, "Special points for Brillouin-zone integrations," *Phys. Rev. B,* Vol.13, 1972, 5188.

37. L.-G. Liu, "Compression and polymorphism of potassium to 400 kbar," *J. Phys. Chem. Solids,* Vol.47, 1986, 1067-1072.

38. E. Aruja and H. Perlitz, "Neubestimmung der Gitterkonstante von Natrium," *Z. Kristallogr. Kristallgeom. Kristallphys. Kristallchem.,* Vol.100, 1939, 195-200.

39. R. Hultgren, R. L. Orr, P. D. Anderson and K. K. Kelley, *Selected Values of Thermodynamic Properties of Metals and Alloys,* Wiley, New York, 1963.

40. F. Laves and H. J. Wallbaum, "Influence of geometric factors on the stochimetric formula of metallic compounds shown in the crystal structure of KNa," *Z. Anorg. Chem.,* Vol.250, 1942, 110-120.

41. K. Ozturk, Y. Zhong, L. Q. Chen, C. Wolverton, J. O. Sofo and Z. K. Liu, "Linking first-principles energetics to CALPHAD: An application to thermodynamic modeling of the Al-Ca binary system," *Metall. Trans. A,* Vol.36A, 2005, 5-13.

42. P. Liang, H. L. Su, P. Donnadieu, M. G. Harmelin, A. Quivy, P. Ochin, G. Effenberg, H. J. Seifert, H. L. Lukas and F. Aldinger, "Experimental investigation and thermodynamic calculation of the central part of the Mg-Al phase diagram," *Z. Metallk.,* Vol.89, 1998, 536-540.

43. J. Grobner, R. Schmid-Fetzer, A. Pisch, C. Colinet, V. V. Pavlyuk, G. S. Dmytriv, D. G. Kevorkov and O. I. Bodak, "Phase equilibria, calorimetric study and thermodynamic modeling of Mg--Li--Ca alloys," *Thermochim. Acta,* Vol.389, 2002, 85-94.

44. C. T. Heycock and F. H. Neville, "The Lowering of the Freezing Point of Sodium by the Addition of other Metals," *J. Chem. Soc.,* Vol.55, 1889, 666-676.

45. C. H. Mathewson, "Sodium-Aluminum, Sodium-Magnesium, and Sodium-Zinc Alloys," *Z. Anorg. Chem.,* Vol.48, 1906, 191-193.

46. E. Scheuer, "Study of the Solubility of Sodium in Aluminium," *Z. Metallk.,* Vol.27, 1935, 83-85.

47. J. L. Murray, "The Al--Na (Aluminum--Sodium) System," *Bull. Alloy Phase Diag.,* Vol.4, 1983, 407-410.

48. W. L. Fink, L. A. Willey and H. C. Stumpf, "Equlibium Relations in Aluminum-Sodium Alloy of High Purity," *Trans. AIME.,* Vol.175, 1948, 364-371.

49. C. E. Ransley and H. Neufeld, "The Solubility Relationships in the Aluminum-Sodium and Aluminum-Silicon-Sodium Systems," *Jpn. Inst. Met.,* Vol.78, 1950, 25-46.

50. S. G. Hansen, J. K. Tuset and G. M. Haarberg, "Thermodynamics of liquid Al-Na alloys determined by using CaF2 solid electrolyte," *Metall. Mater. Trans. B,* Vol.33B, 2002, 577-588.

51. K. Motzfeldt, "Discussion of "The solubility of sodium in liquid aluminum"," *Metall. Mater. Trans. B,* Vol.34B, 2003, 744-746.

52. G. Kaptay, "Discussion of "Thermodynamics of liquid Al-Na alloys determined by using CaF2 solid electrolyte"," *Metall. Mater. Trans. B,* Vol.35B, 2004, 393-398.

53. S. G. Hansen, J. K. Tuset and G. M. Haarberg, "Discussion of "The solubility of sodium in liquid aluminum" - Reply," *Metall. Mater. Trans. B,* Vol.34B, 2003, 746-748.

54. S. G. Hansen, J. K. Tuset and G. M. Haarberg, "Discussion of "Thermodynamics of liquid Al-Na alloys determined by using CaF2 solid electrolyte" - Reply," *Metall. Mater. Trans. B,* Vol.35B, 2004, 398-400.

55. P. Fellner, M. Korenko and V. Danielik, "Comments on the Solubility and Activity of Sodium in Molten Aluminium," A. Solheim, G. M. Haarberg, Eds., *The International Jomar Thonstad Symposium*, Trondheim, Norway, October 16-18, 2002, pp. 199-206.

56. P. Fellner, M. Korenko, V. Danielik and J. Thonstad, "The content of sodium in aluminium during electrolysis of the molten systems Na3AlF6-NaCl-Al2O3 and NaF-NaCl," *Electrochim. Acta,* Vol.49, 2004, 1505-1511.

57. S. G. Hansen, "Personal Communication," *Personal Communication*, 2004

58. J. C. Mitchell and C. S. Samis, "Activity of Sodium in Na-Al System and NaF and AlF3 Activities in NaF-AlF3 Melts," *Trans. TMS-AIME.,* Vol.245, 1969, 1227-1234.

59. E. W. Dewing, "Thermodynamics of the system NaF-AlF3, 1: The Equilibrum 6NaF(s)+Al=Na3AlF6(s)+3Na," *Metall. Trans.,* Vol.1, 1970, 1691-1694.

60. E. W. Dewing, "Thermodynamics of the system NaF-AlF3, 3: Activities in liquid mixtures," *Metall. Trans.,* Vol.3, 1972, 495-501.

61. R. J. Brisley and D. J. Fray, *Metall. Mater. Trans. B,* Vol.14B, 1983, 435-440.

62. P. C. Yao and D. J. Fray, "Sodium activity determinations in molten 99.5% aluminium using solid electrolytes," *J, Appl. Electrochem.,* Vol.15, 1985, 379-386.

63. M. Sun and S. Yang, "Activity of Sodium in Liquid Aluminium," *Journal of Central-South Institute of Mining and Metallurgy,* Vol.23, 1992, 99-104.

64. A. A. Dubreuil and A. D. Pelton, "Probes for the continuous monitoring of sodium and lithium in molten aluminium," *Light Met.,* 1985, 1197-1205.

65. J. Metzger, "On Calcium Metal," *Liebigs Annalen,* Vol.355, 1907, 141-143.

66. R. Lorenz and R. Winzer, "The Ca-Na Phase Diagram," *Z. Anorg. Chem.,* Vol.179, 1929, 281-286.

67. R. Lorenz and R. Winzer, "The Equilibium Between Ca and Na with Their Chlorides," *Z. Anorg. Chem.,* Vol.181, 1929, 193-202.

68. E. Rinck, "Solidification Diagram of Ca-Na Alloys," *Compt. Rend.,* Vol.192, 1931, 1378-1381.

69. A. D. Pelton, "The Ca--Na (Calcium--Sodium) System," *Bull. Alloy Phase Diag.,* Vol.6, 1985, 35-37.

70. M. A. Joannis, "Sub Les Alliages Du Potassium Et Du Sodium," *Ann. Chem. Phys.,* Vol.12, 1887, 358-384.

71. N. S. Kurnakow and N. A. Puschin, "Uber die Schmelztemperaturen der legierungen des Natrium mit Kalium (Germany)," *Z. Anorg. Chem.,* Vol.30, 1902, 109-112.

72. K. Bornemann, "Binary alloy systems," *Metallurgie,* Vol.6, 1909, 239-243.

73. G. L. C. M. v. R. H. v. Bleiswijk, "Uber das Zustandsdiagramm der Kalium-Natriumlegierungen (Germany)," *Z. Anorg. Chem.,* Vol.74, 1912, 152-156.

74. E. Janecke, "Uber die legierungen von Na-K-Hg-Cd (Germany)," *Z. Metallk.,* Vol.20, 1928, 113-117.

75. E. Rinck, "Giagrammes de Solidification des Alliaged Formes Pardeux Metaux Alcalins. Alliqges Sodium-Potassium (Germany)," *Compt.Rend.,* Vol.197, 1933, 49-51.

76. J. B. Ott, J. R. Goates, D. R. Anderson and H. T. Hall, Jr., "Solid-Liquid Phase Equilibria in the Sodium + Potassium System," *Trans. Fara. Soc.,* Vol.65, 1969, 2870-2878.

77. D. K. C. MacDonald, W. B. Pearson and T. Towle, "An Investigation of the Sodium-Potassium Equilibrium Diagram," *Can. J. Phys.,* Vol.34, 1956, 389-394.

78. L. Rimai and H. Bloembergen, "Nuclear magnetic resonance in alkali alloy systems, NaK and NaRb," *J. Phys. Chem. Solids.,* Vol.13, 1960, 257-270.

79. C. A. Krier, R. S. Craig and W. E. Wallace, "Low Temperature Heat Capacities and Related Properties of Potassium and Na2K," *J. Phys. Chem.,* Vol.61, 1957, 522-529.

80. F. R. Bichowsky and F. D. Rossini, *Thermochemistry of Chemical Substances,* Reinhold Publishing Corp., New York, 1936.

81. M. Kawakami, "The Science Reports of the Tohoku Imperial University . First series, (Mathematics, Physics, Chemistry)," *Sci. Rept. Tohoku Univ. First Ser.,* Vol.16, 1927, 915-935.

82. R. L. McKisson and L. A. Bromley, "Heat of formation of Sodium Potassium Alloys," *J. Am. Chem. Soc.,* Vol.73, 1951, 314-315.

83. T. Yokokawa and O. J. Kleppa, "Heats of Mixing in Binary-Liquid-Alkali-Metal Mixtures," *J. Chem. Phys.,* Vol.40, 1964, 46-54.

84. F. A. Cafasso, V. M. Khanna and H. M. Feder, "Thermodynamic Properties and Ordering in Liquid NaK Alloys - Advanced Physics," *International conference on the properties of liquid metals*, 19-23 September 1966, 1967, pp. 535-543.

85. D. N. Kagan, "Measurement of the Activity of Components in Molten Systems of Alkali Metals by the Effusion Method on Electron-Beam Equipment. Analysis of the Technique, Results, Discussion," *Teplofiz. Vys. Temp.,* Vol.26, 1988, 478-491.

86. E. P. Lokshin and O. S. Ignatov, "Activity of the Components of Binary Alloys of Alkali Metals: Na–K System," *Teplofiz. Vys. Temp.,* Vol.9, 1971, 94-98.

87. M. F. Lantratov, "Thermodynamic Proporties of Na-Mg and K-Mg Molten Alloys," *J. Appl. Chem. USSR.,* Vol.46, 1973, 2107-2110.

88. E. E. Shpil'rain, V. I. Shkermontov, S. N. Skovorod'ko and A. G. Mozgovoi, "Activity of the components of binary alloys of alkali metals: Na-K system," *High Temp.,* Vol.40, 2002, 33-43.

89. H. K. Schurmann and R. D. Parks, "Paraconductivity in Binary Metallic Liquids above the Critical Point," *Phys. Rev. Lett.,* Vol.27, 1971, 1790-1793.

90. M. G. Feistma, J. J. Hallers, F. V. D. Werff and W. V. Lugt, "Electrical Resistivities and Phase Separation of Liquid Lithiun-Sodium Alloys," *Pysica B,* Vol.79, 1975, 35-52.

91. M. G. Down, P. Hubberstey and R. J. Pulman, "Sodium-Lithium Phase Diagram: Redetermination of the Liquid Immiscibility System by Resistance Measurement," *J. Chem. Soc. Dalton Trans.,* Vol.14, 1975, 1490-1492.

92. M. G. Down, P. Hubberstey and R. J. Pulman, "Electrical Resistivity of Liquid Sodium + Lithium Mixtures-Evidence of Incipient Immiscibility," *JCS Faraday I,* Vol.71, 1975, 1387-1391.

93. H. Endo, H. Hoshino, K. Tamura and M. Mushiage, "Phase separation of liquid binary mixtures containing metals under pressure," *Solid State Sci.,* Vol.32, 1979, 1243-1246.

94. F. A. Kandan, R. C. Faxon and D. V. Keller, "The Determination of the Liquid Immiscibility Boundary of the Lithium-Sodium and Thallium-Selenium Systems by the Liquid Density Method," *Phys. Chem. Liquids,* Vol.1, 1968, 61-73.

95. E. S. Wu and H. Brumberger, "Critical Small-Angle X-Ray Scatting of the Liquid Solidum-Lithium Alloys," *Phys. Lett. A,* Vol.53, 1975, 475-477.

96. C. W. Bale, "The Li--Na (Lithium--Sodium) System," *Bull. Alloy Phase Diag.,* Vol.10, 1989, 265-268.

97. A. D. Pelton, "Calculation of Phase-Equilibria and Thermodynamic Properties of the Li-Na-H System," *Z. Metallk.,* Vol.84, 1993, 767-772.

98. W. Klemm and D. Kunze, "Systems pf Alkali ans Alkaline Earth Metals," *London Chem. Soc.,* Vol.22, 1967, 3-22.

99. A. D. Pelton, "The Mg-Na System," *Bull. Alloy Phase Diag.,* Vol.5, 1984, 454-456.

100. J. O. Andersson, T. Helander, L. H. Hoglund, P. F. Shi and B. Sundman, "THERMO-CALC & DICTRA, computational tools for materials science," *CALPHAD,* Vol.26, 2002, 273-312.
101. E. W. Dewing, "Thermodynamics of the system NaF-AlF3 .6. Revision," *Metall. Trans. B,* Vol.21B, 1990, 285-294.
102. W. H. Howland and L. F. Epstein, "The Binary System Sodium-Lithium," *Advan.Chem. Ser.,* Vol.19, 1957, 34-41.
103. O. N. Salmon and D. H. Ahmann, "The Lithium-Sodium Liquid Metal System," *J. Phy. Chem.,* Vol.60, 1956, 13-16.
104. C. E. Ransley and D. E. J. Talbot, "THE EMBRITTLEMENT OF ALUMINIUM MAGNESIUM ALLOYS BY SODIUM," *J. Inst. Met.,* Vol.88, 1959, 150-158.
105. M. Otsuka and R. Horiuchi, "Ductility Loss of Al-Mg alloys at High Temperature," *J. Jpn. Inst. Met.,* Vol.48, 1981, 688-693.
106. H. Okada and M. Kanno, "Hot ductility of Al-Mg and Al-Mg-Y alloys impaired by trace sodium," *Scr. Mater.,* Vol.37, 1997, 781-786.
107. S. J. Zhang, Q. Y. Han and Z. K. Liu, "Thermodynamic modeling of the Al-Mg-Na system," *J. Alloy. Compd.,* Vol.419, 2006, 91-97.
108. S. I. Tomkeieff, "Linear intercepts, areas and volumes," *Nature,* Vol.155, 1945, 24.